Mon. Not. R. Astron. Soc. **338,** 555–571 (2003)

Modelling infrared galaxy evolution using a phenomenological approach

G. Lagache,[1]★ H. Dole[2] and J.-L. Puget[1]

[1]*Institut d'Astrophysique Spatiale, Bât. 121, Université Paris XI, 91405 Orsay Cedex, France*
[2]*Steward Observatory, University of Arizona, 933 N. Cherry Ave, Tucson, AZ 85721, USA*

Accepted 2002 August 9. Received 2002 August 9; in original form 2002 June 6

ABSTRACT

To characterize the cosmological evolution of the sources contributing to the infrared extragalactic background, we have developed a phenomenological model that constrains in a simple way the evolution of the galaxy luminosity function with redshift, and fits all the existing source counts and redshift distributions, cosmic infrared background intensity and fluctuation observations, from the mid-infrared to the submillimetre range. The model is based on template spectra of starburst and normal galaxies, and on the local infrared luminosity function. Although the cosmic infrared background can be modelled with very different luminosity functions as long as the radiation production with redshift is the right one, the number counts and the anisotropies of the unresolved background imply that the luminosity function must change dramatically with redshift, with a rapid evolution of the high-luminosity sources ($L > 3 \times 10^{11}\,\mathrm{L}_{\odot}$) from $z = 0$ to $z = 1$, which then stay rather constant up to redshift $z = 5$. The derived evolution of the infrared luminosity function may be linked to a bimodal star formation process: one associated with the quiescent and passive phase of the galaxy evolution, and one associated with the starburst phase, triggered by merging and interactions. The latter dominates the infrared and submillimetre output energy of the Universe.

The model is intended as a convenient tool to plan further observations, as illustrated through predictions for *Herschel*, *Planck* and ALMA observations. Our model predictions for given wavelengths, together with some useful routines, are available for general use.

Key words: galaxies: evolution – galaxies: general – galaxies: starburst – cosmology: observations – infrared: galaxies.

1 INTRODUCTION

The discovery of the cosmic infrared background (CIB) (Puget et al. 1996; Fixsen et al. 1998; Hauser et al. 1998; Schlegel, Finkbeiner & Davis 1998; Lagache et al. 1999, 2000; see Hauser & Dwek 2001 for a review), together with recent deep cosmological surveys in the infrared (IR) and submillimetre, has opened new perspectives on our understanding of galaxy formation and evolution. The surprisingly high amount of energy contained in the CIB showed that it is crucial to probe its contributing galaxies to understand when and how the bulk of stars formed in the Universe. Thanks to *ISO* (Kessler et al. 1996) – mainly at 15 μm with ISOCAM (Cesarsky et al. 1996), and at 90 and 170 μm with ISOPHOT (Lemke et al. 1996) – and ground-based instruments – SCUBA (Holland et al. 1998) and MAMBO (Bertoldi et al. 2000) at 850 and 1300 μm respectively – deep cosmological surveys have been carried out. It is thus now possible, to various degrees, to resolve the CIB into discrete sources (e.g. Kawara et al. 1998; Barger, Cowie & Sanders 1999; Elbaz et al. 1999; Carilli et al. 2001; Juvela, Mattila & Lemke 2000; Linden-Vornle et al. 2000; Matsuhara et al. 2000; Bertoldi et al. 2000; Dole et al. 2001; Elbaz et al. 2002; Scott et al. 2002). The striking result of these surveys concerns the evolution of the IR and submillimetre galaxy population. The source counts are high when compared to no-evolution or moderate-evolution models[1] for IR galaxies (Guiderdoni et al. 1998; Franceschini, Andreani & Danese 1998). Therefore, it has been necessary to develop new models in the IR. Very recently, several empirical approaches have been proposed to model the high rate of evolution of IR galaxies (e.g. Devriendt & Guiderdoni 2000; Wang & Biermann 2000; Charry & Elbaz 2001; Franceschini et al. 2001; Malkan & Stecker 2001; Pearson 2001; Rowan-Robinson 2001; Takeuchi et al. 2001; Xu et al. 2001; Balland, Devriendt & Silk 2002; Wang 2002), which fit all existing source counts, redshift distributions, and CIB intensity and fluctuations, although often not all of them. We present in this paper a new model whose preliminary results were published by Dole et al.

★E-mail: guilaine.lagache@ias.u-psud.fr

[1] No-evolution: the comoving luminosity function remains equal to the local one at all redshifts.

(2000). The originality of this model was to separate empirically the evolution of the starburst galaxies with respect to the normal galaxies, the current observations implying a strong evolution of the bright part of the luminosity function (LF). It was shown that only the starburst part should evolve very rapidly between $z = 0$ and $z = 2$, the evolution rate being much higher in the IR than in any other wavelength domain.

We present here a more sophisticated and detailed version of the first model (Dole et al. 2000). Our philosophy is to build the simplest model of LF evolution, easily deliverable, with the lowest number of parameters but accounting for all observational data. We stress the point that we include the CIB fluctuation levels as measured by ISOPHOT (Lagache & Puget 2000; Matsuhara et al. 2000) and *IRAS* (Miville-Deschênes, Lagache & Puget 2002) as an extra constraint. Recent observations strongly suggest that the bulk of the optical and IR extragalactic background is made of two distinct galaxy populations (see Section 2.2). Therefore, we restrict our model to the wavelength domain 10–1500 μm, our goal being to quantify the evolution of IR galaxies.

The paper is organized as follows: we first summarize our present knowledge on the evolution of IR galaxies, and on the nature of the sources contributing to the extragalactic background (Section 2). Then, we present the ingredients of the model (Section 3). In Section 4, we discuss the galaxy templates used in the model. We then present the parametrization of the local LF (Section 5). In Section 6 are given the results of the model (evolution of the LF, evolution of the luminosity density, number counts, z distribution, CIB intensity and fluctuations). Finally the model is used for predictions for the *Herschel* and *Planck* surveys (Sections 7.2 and 7.3 respectively), gives requirements for future large deep survey experiments (Section 7.4) and predictions for ALMA observations (Section 7.5). A summary is given in Section 8.

2 OUR PRESENT KNOWLEDGE

2.1 The strong evolution of IR galaxies: observational evidence

There has been, in the past few years, strong observational evidence indicating extremely high rates of evolution for IR galaxies.

First, galaxy evolution can be observed through its imprint on the far-IR extragalactic background (EB). Weakly constrained even as recently as 6 yr ago, various observations now measure or give upper/lower limits on the background from the ultraviolet (UV) to the millimetre waveband (e.g. Dwek et al. 1998; Gispert, Lagache & Puget 2000; Hauser & Dwek 2001). The data show the existence of a minimum between 3 and 10 μm separating direct stellar radiation from the IR part due to radiation re-emitted by dust. This re-emitted dust radiation contains at least a comparable integrated power as the optical/near-IR, and perhaps as much as 2.5 times more. This ratio is much larger than what is measured locally (∼30 per cent). The CIB is thus likely to be dominated by a population of strongly evolving redshifted IR galaxies. Since the long-wavelength spectrum of the background is significantly flatter than the spectrum of local star-forming galaxies, it strongly constrains the far-IR radiation production rate history (Gispert et al. 2000). The energy density must increase by a factor larger than 10 between the present time and redshift $z \sim 1$–2 and then stay rather constant at higher redshift (till ∼3), contrary to the ultraviolet radiation production rate, which decreases rapidly.

Secondly, several deep cosmological surveys at 15, 90, 170, 850 and 1300 μm have resolved a fraction of the CIB into discrete sources. For all surveys, number counts indicate a very strong cosmological evolution of IR galaxies, not only in total power radiated but also in the shape of the LF. This is particularly obvious at submillimetre wavelengths where the EB is dominated by high-luminosity galaxies (see the SCUBA and MAMBO results). The high rates of evolution exceed those measured in other wavelength domains as well as those observed for quasars and active galactic nuclei (AGNs).

Finally, high rates of evolution are suggested by the detection of Poissonian fluctuations of the CIB at a high level at 60 and 100 μm with *IRAS* (Miville-Deschênes et al. 2002) and 170 μm with ISOPHOT (Lagache & Puget 2000; Matsuhara et al. 2000). For example, Matsuhara et al. (2000) give the constraints on the galaxy number counts down to 35 mJy at 90 μm and 60 mJy at 170 μm, which indicate the existence of a strong evolution down to these fluxes in the counts.

2.2 Sources making the extragalactic background

2.2.1 Optical versus infrared and submillimetre EB sources

Recent observations show that the bulk of the optical and IR EB is made up by two distinct galaxy populations (e.g. Aussel et al. 1999). Therefore, one of the key questions is whether the dusty star-forming galaxies are recognizable from optical/near-IR data alone.

In the local Universe, Sanders & Mirabel (1996) show that the bolometric luminosity of IR galaxies is uncorrelated with optical spectra. The colour excess derived from the Balmer line ratio does not significantly depend on the IR luminosity, IR colour or optical spectral type (Veilleux, Kim & Sanders 1999). In fact, neither the moderate strength of the heavily extinguished starburst emission lines, nor their optical colours, can distinguish them from galaxies with more modest rates of star formation (Elbaz et al. 1999; Trentham, Kormendy & Sanders 1999; Poggianti et al. 1999). However, recently, Poggianti & Wu (2000) and Poggianti, Bressan & Franceschini (2001) show that the incidence of e(a)[2] sources in the different IR-selected samples seems to suggest that the e(a) signature might be capable of identifying from optical data alone a population of heavily extinct starburst galaxies. Reproducing the e(a) spectrum requires the youngest stellar generations to be significantly more extinguished by dust than older stellar populations, and implies a strong ongoing star formation activity at a level higher than in quiescent spirals.

At intermediate redshift ($0.3 < z < 1$), one main piece of information on IR galaxies comes from identifications of ISOCAM deep fields. For example, Flores et al. (1999a,b) presented results of a deep survey of one of the CFRS fields at 6.75 and 15 μm. At 15 μm, most (71 per cent) of the sources with optical spectroscopy are classified as e(a) galaxies. The far-IR luminosities of the Flores et al. e(a) galaxies are between 5.7×10^{10} and 2×10^{12} $L_{\odot}$. This is the first confirmation of the IR luminous nature of e(a) galaxies. More recently, Rigopoulou et al. (2000) using VLT spectroscopy found that optical ISOCAM counterparts in the *Hubble Deep Field* South (HDF-S) are indistinguishable from the dusty luminous e(a) galaxies.

All these studies at low and intermediate redshift seem to show that IR galaxies predominantly exhibit e(a) signatures in their optical spectra. On the contrary, in optically selected surveys of field galaxies, e(a) spectra are present but seem to be scarce (less than 10 per cent; see for example Poggianti et al. 1999). In fact, evidence

[2] Galaxies with strong Balmer absorption lines and [O II] in emission (Poggianti & Wu 2000, and references therein).

for high e(a) incidences is found in merging or interacting systems or active compact groups. A complete study of the IR emission of e(a) galaxies is still to be done.

At much higher redshift, there is other evidence that the optically selected samples and bright IR samples (e.g. the SCUBA blank field sample) are different. For example, Chapman et al. (2000) have performed submillimetre photometry for a sample of Lyman break galaxies whose UV properties imply high star formation rates. They found that the integrated signal from their Lyman break sample is undetected in the submillimetre. This implies that the population of Lyman break galaxies does not constitute a large part of the detected blank field bright submillimetre sources.

In conclusion, it is clear that the optical and IR EBs are not dominated by the same population of galaxies. Therefore, we restrict our model to the wavelength domain 10–2000 μm, our goal being to quantify the evolution of IR galaxies.

2.2.2 *The CIB sources*

In the *Hubble Deep Field* North (HDF-N), Aussel et al. (1999) and Elbaz et al. (1999) find that 30–50 per cent of ISOCAM galaxies are associated with optical sources showing complex structures and morphological peculiarities. Moreover, Cohen et al. (2000) show, in the HDF-N, that more than 90 per cent of the faint ISOCAM sources are members of concentrations. This shows that past or present interactions or merging play a large role in triggering the IR emission of galaxies. All the studies of ISOCAM field sources show that the bulk of the CIB at 15 μm comes from galaxies that have bolometric luminosities of about 10^{11}–10^{12} $L_\odot$, high masses ($\sim 10^{11}$ $M_\odot$) and redshift between 0.5 and 2. They experience intense stellar formation (100 $M_\odot$ yr^{-1}), which appears to be uncorrelated with the faint blue galaxy population dominating the optical counts at $z \sim 0.7$ (Ellis 1997; Elbaz et al. 1999). In galaxy clusters all ISOCAM sources are found preferably at the periphery where there is still some star formation (Biviano, Metcalfe & Altieri 1999).

At longer wavelengths, source identifications are much more difficult. Thus, characterizing the nature of the galaxies is a lengthy process. However, we already have some indications. The *FIRBACK* survey at 170 μm detected about 200 galaxies (Dole et al. 2001), making up less than 10 per cent of the CIB. Schematically *FIRBACK* sources comprise two populations: one cold and nearby ($L \sim 10^9$–10^{11} $L_\odot$), and one cold or warm very luminous ($L \sim 10^{12}$ $L_\odot$) with redshift lower than 1.2. The optical spectroscopy of the brightest *FIRBACK* sources reveals an '*IRAS*-like' starburst nature (Patris et al. 2002; Dennefeld et al., in preparation) with a moderate star formation rate (40 $M_\odot$ yr^{-1}). These results are very similar to those of Kakazu et al. (2002), who found that 62 per cent of the Lockman Hole 170-μm sources are at redshift below 0.3 with luminosities lower than 10^{12} $L_\odot$ (based on the spectrum of Arp 220), the rest being mostly ultraluminous IR galaxies with redshift between 0.3 and 1. In their sample, the 170-μm sources appear also to be powered primarily by star formation.

In the submillimetre, the main indication comes from the SCUBA deep surveys (e.g. Hughes et al. 1998; Barger et al. 1999; Eales et al. 1999; Scott et al. 2002). These surveys suggest that faint 850-μm sources are mostly ultraluminous galaxies at typical redshift between 1 and 4 (e.g. Eales et al. 2000). *SCUBA* sources above 3 mJy account for 20–30 per cent of the EB at 850 μm. The present data show that the bulk of the submillimetre EB is likely to reside in sources with 850-μm fluxes near 0.5 mJy. Barger et al. (1999) estimate that the far-IR luminosity of a characteristic 1-mJy source is in the range (4–5) $\times$ 10^{11} $L_\odot$, which is also typical of sources making up the bulk of the CIB at 15 μm. Moreover, as for the 15-μm sources, several groups have suggested that the submillimetre sources are associated with merger events (e.g. Smail et al. 1998; Lilly et al. 1999). All these results show that the integrated power of the LF at redshift greater than ~ 0.5 must be dominated by sources with luminosities of a few 10^{11} $L_\odot$ while the local LF is dominated by sources with luminosities of the order of 5×10^{10} $L_\odot$.

2.2.3 *The AGN contribution to the IR output energy*

At low z, Veilleux et al. (1999) and Lutz et al. (1999) show that most of the IR sources are powered by starbursts. The AGN contribution appears dominant only at very high luminosities ($L > 2 \times 10^{12}$ $L_\odot$). Also using *FIRBACK* nearby bright source spectroscopy, we find that less than 10 per cent of sources show AGN signs (Patris et al. 2002; Dennefeld et al., in preparation). The same conclusions are reached by Kakazu et al. (2002). At intermediate z, from optical and X-ray studies of ISOCAM sources making up the bulk of the CIB, several groups show that 15-μm sources are mostly starburst galaxies (e.g. Fadda et al. 2002). At much higher z, the main indication comes from X-ray observations of SCUBA sources (Fabian et al. 2000; Hornschemeier et al. 2000; Severgnini et al. 2000; Barger et al. 2001). All these observations of submillimetre galaxies in X-rays are consistent with starburst-dominated emission. However, recently, Page et al. (2002) presented a result of SCUBA observations of eight X-ray absorbed AGN from $z = 1$ to 2.8 and find, for half of them, a 850-μm submillimetre counterpart. Nevertheless, the high 850-μm fluxes (greater than 5.9 mJy) suggest that these sources are hyperluminous galaxies. Such galaxies do not dominate the IR output of the Universe.

Considering the whole CIB energy budget, and based on the assumptions that 10 per cent of the mass accreting into a black hole is turned into energy and that the black hole masses measured in the HDF (Ford et al. 1998) are typical of galaxies, the AGN background energy would be of the order of 10 per cent of that from stars (Eales et al. 1999). These calculations are highly uncertain but are supported by the work of Almaini, Lawrence & Boyle (1999). Recently, more direct evidence has been obtained. For example, Severgnini et al. (2000) show that the 2–10 keV sources making up at least 75 per cent of the X-ray background in this band contribute less than 7 per cent to the submillimetre background.

On the modelling side, several groups (e.g. Xu et al. 2001; Rowan-Robinson 2001) have shown that starburst galaxies evolve much more rapidly than AGN-dominated sources, making the AGN contribution to the CIB relatively small.

In conclusion, it is clear that AGNs do not dominate the IR output energy of the Universe. Therefore, we will consider hereafter that IR galaxies are mostly powered by star formation and we use spectral energy distributions (SED) typical of these star-forming galaxies. The differences in SED for the small fraction of AGN-dominated IR galaxies would not significantly affect the results of our model, which is made up of only two galaxy populations ('normal' and starburst) defined by their SEDs.

3 INGREDIENTS OF THE MODEL

At a given wavelength $\lambda = \lambda_0$, the flux S_ν of a source at redshift z, as a function of the rest-frame luminosity L_ν (in W Hz^{-1}), can be written as

$$S_\nu(L, z, \lambda = \lambda_0) = \frac{(1+z)\,k(L,z)\,L_\nu(L, \lambda = \lambda_0)}{4\pi\, D_{\rm L}^2}, \quad (1)$$

where $D_{\rm L}$ is the luminosity distance and $k(L, z)$ is the k-correction factor defined as

$$k(L, z) = \frac{L_{\nu(1+z)}}{L_{\nu(z=0)}}. \quad (2)$$

This correction is specific to the spectrum of the considered population at given L and z. In practice, the rest-frame luminosity L_ν is convolved by the bandpass filter centred on $\lambda = \lambda_0$. The number of sources per solid angle and redshift interval is

$$\frac{{\rm d}N}{{\rm d}z\,{\rm d}\log L}(L, z) = N_0(L, z)\,(1+z)^3\,\frac{{\rm d}V}{{\rm d}z}, \quad (3)$$

where ${\rm d}V/{\rm d}z$ is the differential volume element fixed by the cosmology and N_0 is the number of sources per unit volume and luminosity interval as a function of redshift. N_0 is given by the LF.

The differential counts at a given flux S and wavelength $\lambda = \lambda_0$ can be written as

$$\frac{{\rm d}N}{{\rm d}S} = \int_L \int_z \frac{{\rm d}N}{{\rm d}z\,{\rm d}\log L}(L, z)\,\frac{{\rm d}z}{{\rm d}S}(L, z)\,{\rm d}\log L. \quad (4)$$

We then obtain the integral counts,

$$N(>S) = \int \frac{{\rm d}N}{{\rm d}S}\,{\rm d}S, \quad (5)$$

the CIB intensity produced by all sources with $S < S_{\rm max}$,

$$I_{\rm CIB} = \int_0^{S_{\rm max}} S\,\frac{{\rm d}N}{{\rm d}S}\,{\rm d}S, \quad (6)$$

and the CIB intensity fluctuations (the shot noise) from sources below a given detection limit S_0 (which could correspond to either the confusion or the sensitivity limit) measured by the level of the white noise power spectrum,

$$P_{\rm fluc} = \int_0^{S_0} S^2\,\frac{{\rm d}N}{{\rm d}S}\,{\rm d}S\ {\rm Jy}^2\ {\rm sr}^{-1}. \quad (7)$$

We build the simplest model with the lowest number of parameters and ingredients which fits all the observations. We first fix the cosmology ($\Omega_\Lambda = 0.7$, $\Omega_0 = 0.3$ and $h = 0.65$) from the combination of the most recent cosmic microwave background (CMB) anisotropy measurements (e.g. de Bernardis et al. 2002), the distance–luminosity relation of Type Ia supernovae (e.g. Perlmutter et al. 1999) and the measure of galaxy distances using Cepheids (e.g. Freedman et al. 2001). We then construct the 'normal' and starburst template spectra: at each population and luminosity is associated one spectrum (see Section 4). We finally search for the best evolution of the LF (equation 3) that reproduces the number counts (equations 4 and 5), the CIB and its fluctuations (equations 6 and 7 respectively), assuming that the LF evolution is represented by the independent evolution of the two populations. A rather remarkable result, as will be seen later, is that two populations only can fit all the data.

4 BUILDING GALAXY TEMPLATES

4.1 Starburst galaxies

The luminous IR starburst galaxies emit more than 95 per cent of their energy in the far-IR. Spectra of such galaxies have been modelled by Maffei (1994), using the Désert, Boulanger & Puget (1990) dust emission model and the observational correlation for the *IRAS* Bright Galaxy Sample of the flux ratios 12/60, 25/60 and 60/100 with the IR luminosity (Soifer & Neugebauer 1991). We start from this model and modify it slightly to better take into account recent observational constraints. The significant improvements are the following:

(i) We replace the Désert et al. (1990) polyaromatic hydrocarbons (PAHs) template by the Dale et al. (2001) one, keeping the same amount of energy in the mid-IR.

(ii) We slightly modify the spectral shape in the near- and mid-IR: we increase the PAH and very small grains proportions (by a factor ~2) but add some extinction, slowly increasing with the luminosity.

(iii) Finally, we broaden the far-IR peak (also a continuous change with luminosity) and slightly flatten the long-wavelength spectrum (Dunne et al. 2000; Dunne & Eales 2001; Klaas et al. 2001).

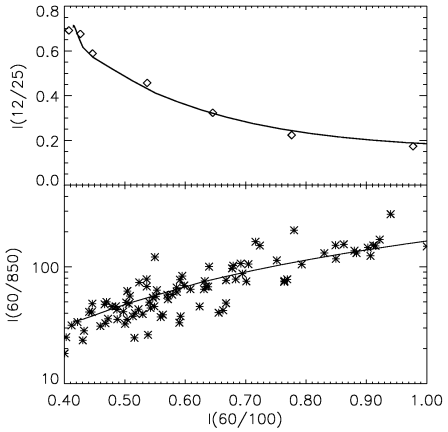

Figure 1. Colour diagrams from the model (full lines), compared with Soifer & Neugebauer (1991) (diamonds) and Dunne et al. (2000) (stars) data points.

Fig. 1 shows the (12/25, 60/100) and (60/850, 60/100) colour diagrams compared with Soifer & Neugebauer (1991) and Dunne et al. (2000) observations. We see a very good agreement between the templates and observations. The average luminosity spectra sequence is shown in Fig. 2. For the 'normal' starbursting galaxies ($L_{\rm IR} < 10^{11}\ {\rm L}_\odot$), we also check that the 7/15 versus 60/100 diagram was in good agreement with Dale et al. (2001).

Such a representation of galaxy SEDs that assigns only one spectrum per luminosity does not take into account the dispersion of the colours (e.g. the 60/100 ratio) observed for a given luminosity (as in Xu et al. 2001 or Chapman et al. 2002a). However, we do not have enough measured colours to do a statistical analysis of their variations with luminosities. The only colours measured for a large sample are the *IRAS* colours (principally the 60/100). Using only the 60/100 colour as a tracer of the dispersion for a given luminosity may not improve the representation, because, for example, two very different long-wavelength spectra can have the same 60/100 colour (e.g. NGC 7821 and 0549; Stickel et al. 2000).

4.2 Normal spiral galaxies

For the 'normal' galaxies (i.e. standard IR counterparts of spiral galaxies with more than half of their energy output in the optical), we take a unique spectrum derived mainly from the ISOPHOT serendipity survey (Stickel et al. 2000) and the nearby *FIRBACK*

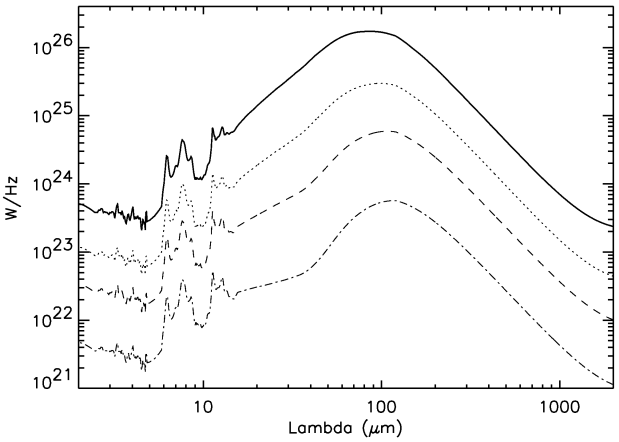

Figure 2. Starburst model spectra for different luminosities: $L = 3 \times 10^{12}$ $L_\odot$ (full line), $L = 5 \times 10^{11}$ $L_\odot$ (dotted line), $L = 10^{11}$ $L_\odot$ (dashed line) and $L = 10^{10}$ $L_\odot$ (dot-dashed line).

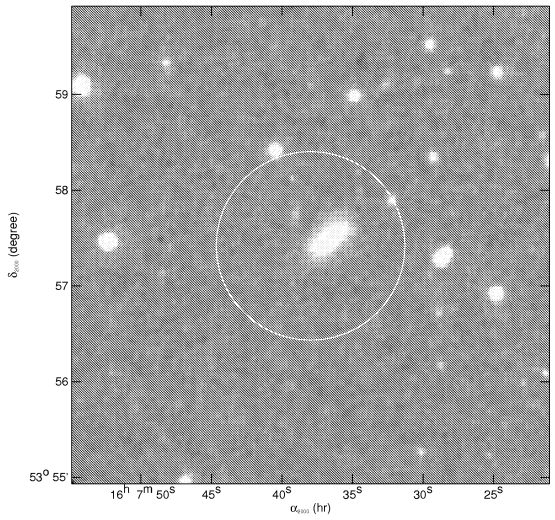

Figure 3. Example of association of one bright *FIRBACK* 170-μm source with a 'cold' spiral galaxy (the optical image is from the DSS; the white circle corresponds to the 170 μm error position). IR colour ratios for this source are $I_{60}/I_{100} = 0.6$, $I_{170}/I_{100} = 1.4$ and $I_{170}/I_{15} = 51$.

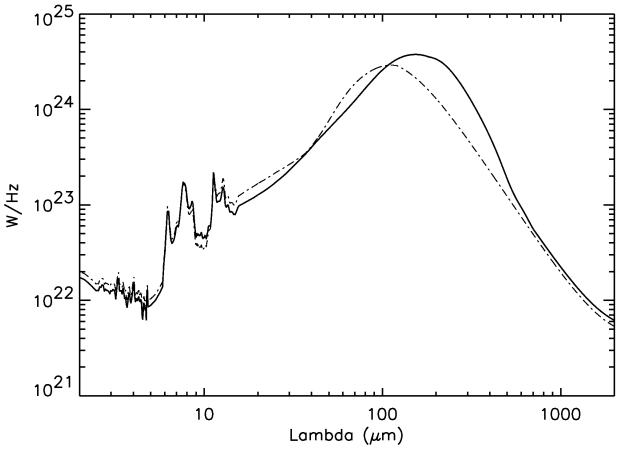

Figure 4. Template spectrum for the normal galaxies (full line), compared with the template spectrum for the starburst galaxies (dot-dashed line), for the same luminosity $L = 5 \times 10^{10}$ $L_\odot$.

galaxy SEDs, together with longer-wavelength data from Dunne et al. (2000) and Dunne & Eales (2001).

The ISOPHOT serendipity survey has revealed a population of nearby cold galaxies (Stickel et al. 1998, 2000), under-represented in the 60-μm *IRAS* sample. The distribution of I_{170}/I_{100} flux ratio shows that about half of the galaxies have a flux ratio between 1 and 1.5, indicating that the far-IR spectra are mostly flat between 100 and 200 μm. Very few show a downward trend in this wavelength range, this trend being typical of warm starburst galaxies (see Fig. 2). Most important is the large fraction of sources (more than 40 per cent) that have $I_{170}/I_{100} > 1.5$, indicating a rising spectrum beyond 100 μm similar to that seen for example in the Milky Way galactic ridge, a property known for more than 20 yr from early balloon-borne measurements (Serra et al. 1978; Silverberg et al. 1979).

In the *FIRBACK* N1 field (Dennefeld et al., in preparation), the brightest sources show mean IR colour similar to that of Stickel et al. (2000): $I_{170}/I_{100} \sim 1.3$ and $I_{60}/I_{100} \sim 0.47$. These objects are often associated with bright optical spiral galaxies (e.g. Fig. 3) with also typical 15-μm fluxes such as $I_{170}/I_{15} \sim 42$. Finally recent observations at 450 μm (Dunne & Eales 2001) reveal also the presence, in normal galaxies, of a colder component than previously thought.

Therefore, we take for the normal galaxy the 'cold' template presented in Fig. 4. This template has mean IR colours of $I_{170}/I_{100} = 1.42$, $I_{60}/I_{100} = 0.35$, $I_{170}/I_{15} = 45$ and $I_{100}/I_{850} = 77$. For the mid-IR part of the template, we use the spectral signature that applies to the majority of star-forming galaxies presented in Helou (2000). More observations around the maximum intensity (∼100–200 μm) and in the submillimetre are needed if we want to refine the template and describe its variations with luminosity.

Note that we do not make any evolution of the 'normal' and starburst template spectra with redshift. As shown in Chapman et al. (2002a), the available data for high-redshift, far-IR galaxies do not show evidence for any strong evolution in the characteristic temperature of the colour distribution over $0 < z < 3$. We can also test this hypothesis of 'no-evolution' using the two high-redshift sources N1-040 and N1-064 detected in the *FIRBACK* N1 field (Chapman et al. 2002b). For these two sources, we do a blind search for both the luminosity and redshift using our template spectra, based on a χ^2 test. For N1-064 the 'normal' and starburst templates give the same χ^2 with $\log(L) = 12.2$ and $z = 0.5$ and $\log(L) = 12.8$ and $z = 1.05$ respectively. The starburst template gives results in good agreement with Chapman et al. (2002b). For N1-040, the best χ^2 is obtained for the 'normal' template with $\log(L) = 12.2$ and $z = 0.45$, which is in perfect agreement with Chapman et al. (2002b). The template spectra give photometric redshifts in good agreement with the spectroscopic redshifts, suggesting no strong evolution of the galaxy SEDs over $0 < z < 1$.

5 PARAMETRIZATION OF THE LOCAL LUMINOSITY FUNCTION

A detailed comparison of the luminosity function of IR-bright galaxies with other classes of extragalactic objects has been made in Sanders & Mirabel (1996). The most striking results are (i) the high-luminosity tail of the IR galaxy LF is clearly in excess of that

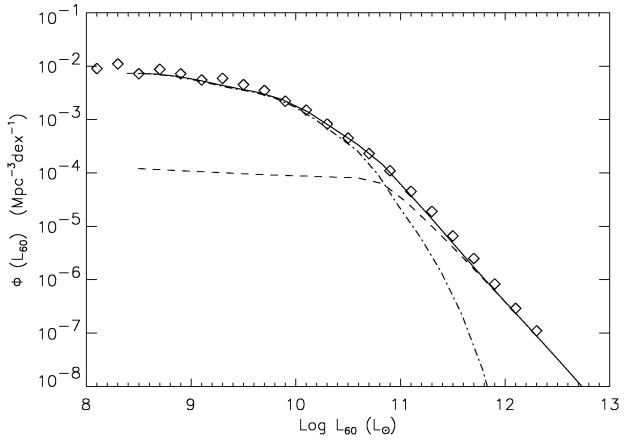

Figure 5. Luminosity function at 60 μm (model: normal galaxies, dot-dashed line; starburst galaxies, dashed line; total, full line) compared with Saunders et al. (1990) (diamonds).

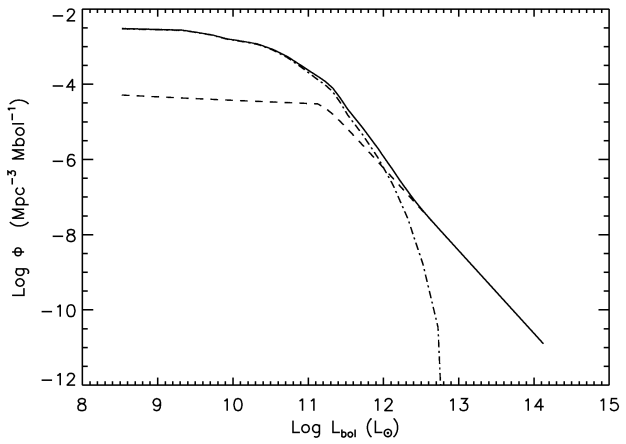

Figure 6. Bolometric luminosity function at $z = 0$ (normal galaxies, dot-dashed line; starburst galaxies, dashed line: total, full line).

expected from a Shechter function, and (ii) at luminosities below $\sim 10^{11}$ $L_\odot$, the majority of optically selected objects are relatively weak far-IR emitters (as shown by *IRAS*, ISOPHOT and SCUBA observations). Accordingly, we decompose the IR LF into two parts: (1) the 'low-luminosity' part (dominated by normal galaxies) that follows the shape of the optical LF, and (2) the 'high-luminosity' part dominated by starburst galaxies (note however that each part covers the whole range of luminosities).

We start from the local LF at 60 μm from Saunders et al. (1990) (Fig. 5). We convert the 60-μm LF into a bolometric LF (L = 1–1000 μm) using our template spectra: at the 'low-luminosity' and 'high-luminosity' part, we assign the 'normal' and starburst template spectra respectively.[3] The bolometric LF (1–1000 μm) used in the model is shown in Fig. 6.

The parametrization and redshift evolution of the two parts of the bolometric LF is done in the following way:

(i) For the normal galaxies:

– A LF at $z = 0$ parametrized by an exponential with a cut-off in luminosity $L_{\rm cut\text{-}off}$

$$\Phi_{\rm normal}(L) = \Phi_{\rm bol}(L)\ \exp\left(\frac{-L}{L_{\rm cut\text{-}off}}\right). \quad (8)$$

– A weak number evolution.

(ii) For the starburst galaxies:

– A LF described by

$$\Phi_{\rm SB}(L, z) = \Phi_{\rm bol}(L = 2.5 \times 10^{11}\,{\rm L}_\odot) \times \left(\frac{L}{2.5 \times 10^{11}\,{\rm L}_\odot}\right)^{\rm SB_{slope}} \exp\left[-\frac{L_{\rm knee}(z)}{L}\right]^3. \quad (9)$$

– An evolution of the luminosity of the knee ($L_{\rm knee}$) with redshift.

– A constant slope of the LF at high luminosities ($\rm SB_{slope}$), not redshift-dependent.

– An evolution of the luminosity density with redshift, $\varphi(z)$, that drives the LF evolution

$$\Phi_{\rm SB}(L, z) = \Phi_{\rm SB}(L, z)\left[\frac{\varphi(z)}{\varphi(z=0)}\right]. \quad (10)$$

– An integrated energy at $z = 0$ as observed: $\rm SB_{norm} = \varphi(z = 0)$.

6 RESULTS AND DISCUSSION

6.1 LF evolution derived from observations

Although the number of parameters is quite low, it is too time-consuming to do a blind search through the whole parameter space. We therefore search for the best solution for the parameters near values expected from direct observational evidence:

(i) We fix the normal galaxy evolution (passive evolution) such that it nearly follows the number density evolution of optical counts up to $z = 0.4$,

$$\Phi_{\rm normal}(L, z) = \Phi_{\rm normal}(L, z = 0)\,(1 + z).$$

We arbitrarily stop the evolution at $z = 0.4$ and keep this population constant up to $z = 5$ and then let the population decrease up to $z = 8$ (see Fig. 8).

(ii) An estimate of $L_{\rm knee}$ is given by deep surveys at 15 and 850 μm: the bulk of the CIB at 15 and 850 μm is made up by galaxies with $L \sim 1$–5×10^{11} $L_\odot$ (e.g. Barger et al. 1999; Elbaz et al. 2002).

(iii) We have indications on the evolution of the luminosity density, $\varphi(z)$, for the starburst galaxies, directly inferred from the CIB spectrum shape by Gispert et al. (2000), which is used as a starting point to adjust the model.

(iv) We take $\rm SB_{norm} = 10^7\,L_\odot\,Mpc^{-3}$, which is roughly the value observed locally.

(v) We take $\rm SB_{slope} = -2.2$ (Kim & Sanders 1998).

The best evolution of the LF that reproduces IR number counts, redshift distributions and CIB observations is shown in Fig. 7. It is obtained with

(i) $L_{\rm cut\text{-}off} = 5 \times 10^{11}$ $L_\odot$.

(ii) $L_{\rm knee}(z) = 8 \times 10^{10}\,(1 + z)^3$ $L_\odot$ up to $z = 1.5$ and then $L_{\rm knee}(z) = L_{\rm knee}(z = 1.5)$.

Moreover, to avoid a 'break' in the evolved luminosity function (as in Dole et al. 2000), we modify the low-luminosity part of the starburst LF with the redshift (up to $z = 5$) according to

$$\Phi_{\rm SB}(L, z) = \Phi_{\rm SB}(L = L_{\rm max}, z) \times \left(\frac{L_{\rm max}}{L}\right)^{(1+z)^2}, \quad (11)$$

[3] We have also checked the validity of the long-wavelength part of our template spectra by comparing the 850-μm LF with Dunne et al. (2000).

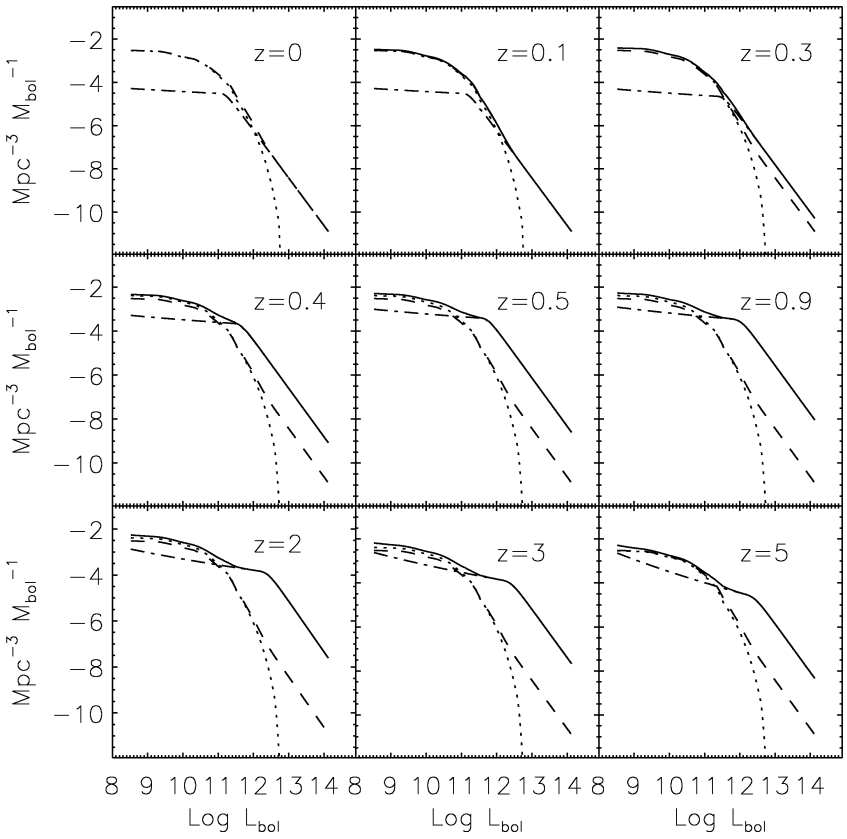

Figure 7. Comoving evolution of the luminosity function. The dotted line is for the normal galaxies and the dot-dashed line is for the starburst galaxies. The full line corresponds to both starburst and normal galaxies, and the dashed line is the LF at $z = 0$ for comparison.

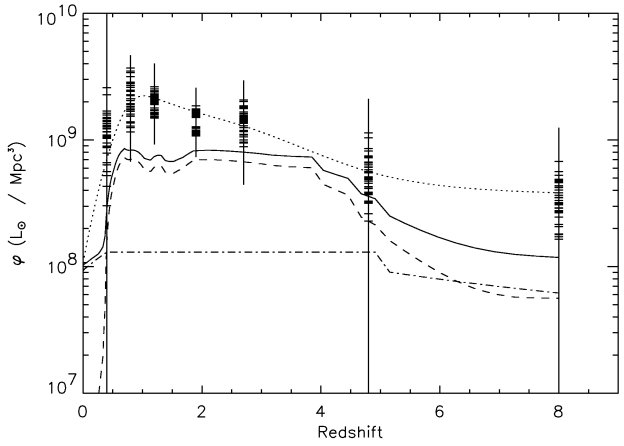

Figure 8. Comoving luminosity density distribution for the starburst galaxies (dashed line), normal galaxies (dot-dashed line), and both normal and starburst galaxies (full line). Also shown for comparison is the comoving luminosity density distribution from all cases of Gispert et al. 2000 (crosses with error bars), together with the best fit passing through all cases (dotted line).

where $L_{\max}$ is the luminosity corresponding to the maximum of $\Phi_{\rm SB}(L, z)$.

We see a very high rate of evolution of the starburst part, which peaks at $z \sim 0.7$ (Fig. 8) and then remains nearly constant up to $z = 4$ (as shown for example by Charry & Elbaz 2001). We compare in Fig. 8 the comoving luminosity density distribution as derived from the model with the Gispert et al. (2000) one. There is a good overall agreement. However, the model is systematically lower than the Gispert et al. (2000) determination for redshifts between 0.5 and 2. This comes from the fact that the CIB values at 100 and 140 μm used in Gispert et al. (2000) were slightly overestimated (Renault et al. 2001), leading in an overestimate of the luminosity density distribution at low redshift.

6.2 Comparison between model and observations

6.2.1 The number counts

Fig. 9 shows the comparison of the number counts at 15 μm (Elbaz et al. 1999), 60 μm (Hacking & Houck 1987; Lonsdale et al. 1990; Saunders et al. 1990; Rowan-Robinson et al. 1990; Gregorich et al. 1995; Bertin, Dennefeld & Moshir 1997), 170 μm (Dole et al. 2001) and 850 μm (Smail et al. 1997; Hughes et al. 1998; Barger et al. 1999; Blain et al. 1999; Borys et al. 2002; Scott et al. 2002; Webb et al. 2002) with the observations. We have a very good overall agreement [we also agree with the 90-μm number counts of Serjeant et al. (2001) and Linden-Vornle et al. (2000)].

6.2.2 The redshift distributions: need for a normal 'cold' population

In Fig. 10 is shown the redshift distribution of resolved sources at 15, 60, 170 and 850 μm. The 15-μm redshift distribution is in very good

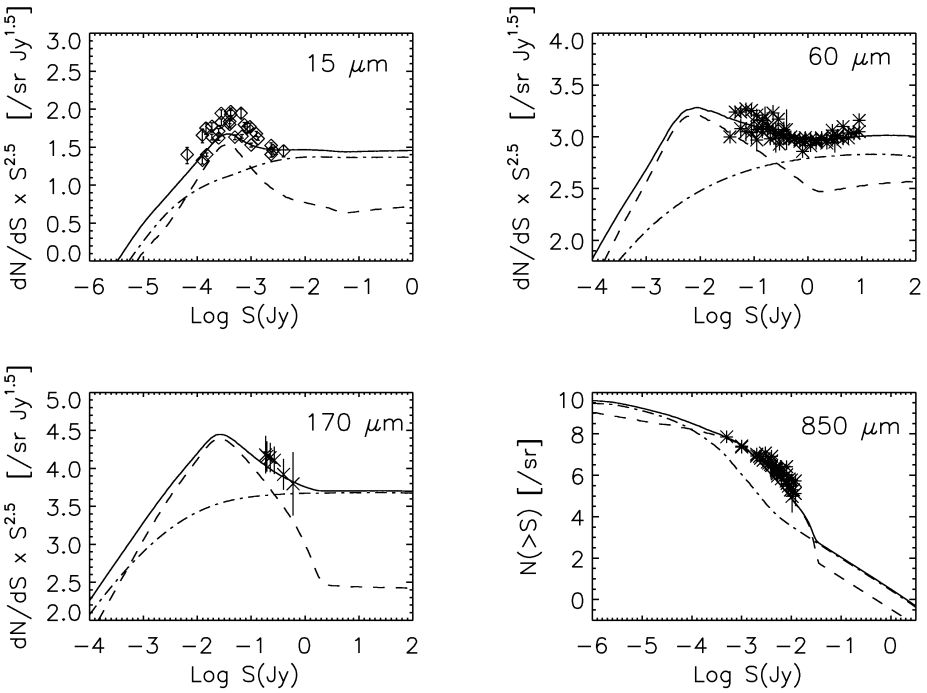

Figure 9. Number counts at 15, 60, 170 and 850 μm (on log scale) together with the model predictions (starburst galaxies, dashed line; normal galaxies, dot-dashed line; both normal and starburst galaxies, full line). Data at 15 μm are from Elbaz et al. (1999), at 170 μm from Dole et al. (2001), at 60 μm from Hacking & Houck (1987), Gregorich et al. (1995), Bertin et al. (1997), Lonsdale et al. (1990), Saunders et al. (1990) and Rowan-Robinson et al. (1990), and at 850 μm from Smail et al. (1997), Hughes et al. (1998), Barger et al. (1999), Blain et al. (1999), Borys et al. (2002), Scott et al. (2002) and Webb et al. (2002).

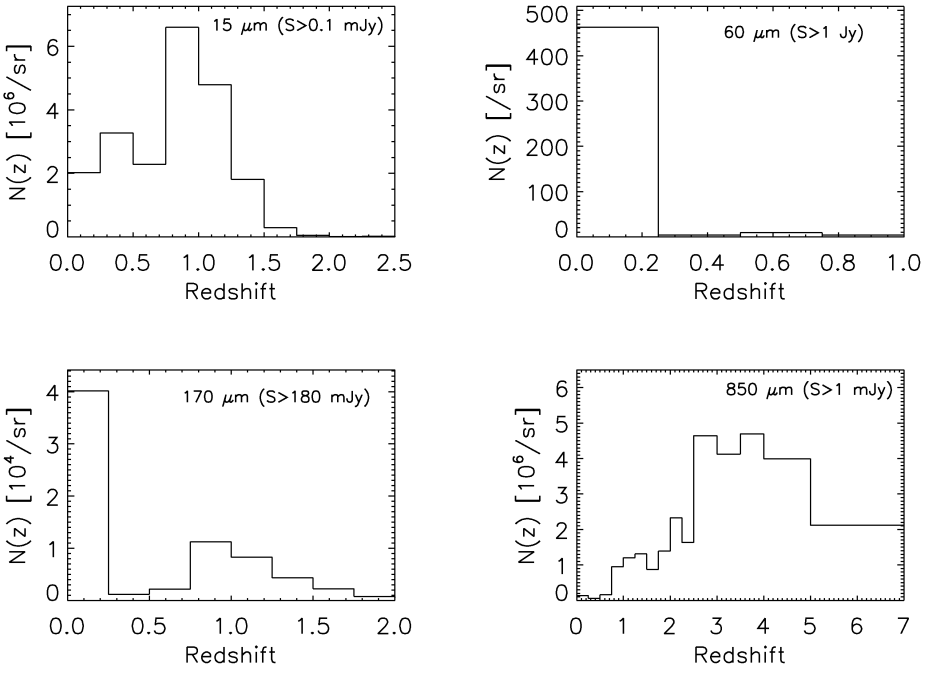

Figure 10. Predicted redshift distribution for resolved sources at 15, 60, 170 and 850 μm.

agreement with that observed by Flores et al. (1999b) and Aussel et al. (1999). At 850 μm, we predict that most of the detected sources are at $z > 2.5$. At 170 μm, we predict that about 62 per cent of sources with fluxes $S > 180$ mJy (4σ in Dole et al. 2001) are at redshift below 0.25, the rest being mostly at redshift between 0.8 and 1.2. We know from the *FIRBACK* observations that the redshift distribution predicted by the model is very close to that observed at 170 μm: it is clear from these observations that we have a bimodal z distribution (Sajina et al. 2002; Dennefeld et al., in preparation). Moreover, very recently, Kakazu et al. (2002) published the first results from optical spectroscopy of 170-μm Lockman Hole sources. They find that 62 per cent of sources are at $z < 0.3$ with IR luminosities (derived using Arp 220 SED) lower than 10^{12} $L_{\odot}$, the rest being at redshift between 0.3 and 1, which is in very good agreement with the model prediction. It is very important to note that the agreement between the model and observations can only be obtained with the local 'cold' population. A model containing only starburst-like template spectra and 'warm' normal galaxies overpredicts by a large factor the peak at $z \sim 1$ (as in Charry & Elbaz 2001, for example).

6.2.3 *The CIB and its anisotropies*

The predicted CIB intensity at specific wavelengths together with the comparison with present observations are presented in Table 1 and in Fig. 11. We have a very good agreement with the estimates at 60 μm (Miville-Deschênes et al. 2002), 100 μm (Renault et al. 2001) and 170 μm (Kiss et al. 2001), and the *FIRAS* determinations (Fixsen et al. 1998; Lagache et al. 2000). We are also in good agreement with the lower limit derived from 15-μm counts (Elbaz et al. 2002), combined with the upper limit deduced from high-energy γ-ray emission of the active galactic nucleus Mrk 501 (Renault et al. 2001). According to the model, sources above 1 mJy at 850 μm contribute about 30 per cent of the CIB. At 15 μm, with the deepest ISOCAM observations (Altieri et al. 1999; Aussel et al. 1999; Metcalfe 2000), about 70 per cent of the CIB has been resolved into individual sources.

Finally, we compare the model predictions for the CIB fluctuations with the present observations at 60, 90, 100 and 170 μm (Table 2). For comparison we need to remove the contribution of the

Table 1. Predicted CIB intensity at 15 μm (ISOCAM filter), 60 and 100 μm (*IRAS* filters), 170 μm (ISOPHOT filter), 350 μm (filter such as $\Delta\lambda/\lambda = 1/3$) and 850 μm (SCUBA filter) compared to measurements.

λ (μm)	Predicted CIB (MJy sr^{-1})	Predicted CIB (W m^{-2} sr^{-1})	Measured CIB (W m^{-2} sr^{-1})	Ref.
15	1.25×10^{-2}	2.5×10^{-9}	$>2.4 \pm 0.5 \times 10^{-9}$	(1)
60	0.12	6.1×10^{-9}	–	
100	0.35	1.1×10^{-8}	$\sim 1.5 \times 10^{-8}$	(2)
170	0.76	1.3×10^{-8}	$1.4 \pm 0.3 \times 10^{-8}$	(3)
350	0.76	6.5×10^{-9}	$5.63^{+4.30}_{-2.80} \times 10^{-9}$	(4)
850	0.20	6.9×10^{-10}	$5.04^{+4.31}_{-2.61} \times 10^{-10}$	(4)

(1) Elbaz et al. (2002).
(2) Renault et al. (2001).
(3) From Kiss et al. (2001) and extrapolation of DIRBE measurements.
(4) From Fixsen et al. (1998) and Lagache et al. (1999).

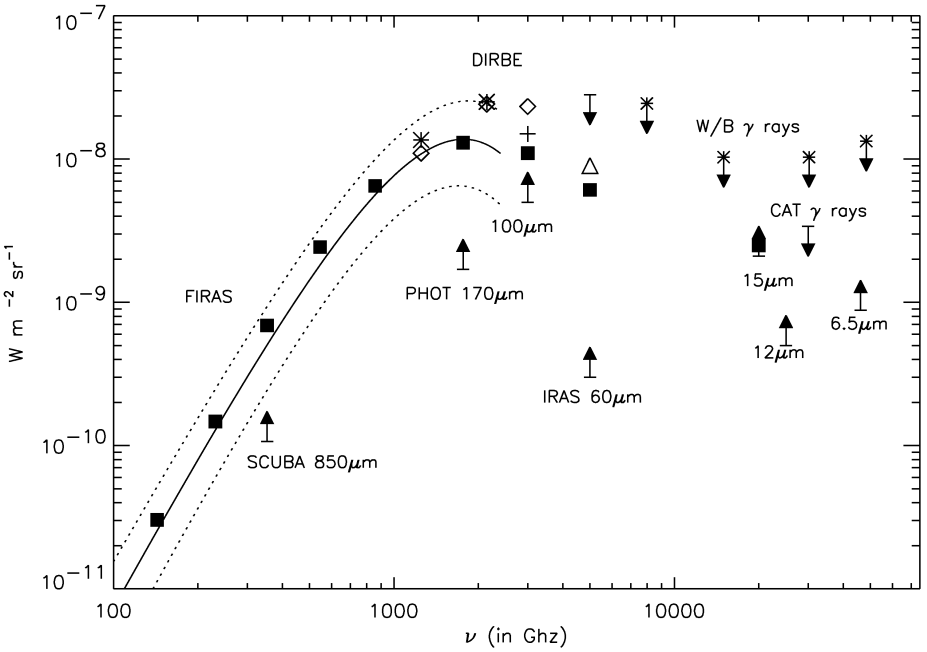

Figure 11. Cosmic background from mid-IR to millimetre wavelength. The 6.5 μm (Désert, private communication), 12 μm (Clements et al. 1999) and 15 μm (Elbaz et al. 2002) lower limits come from ISOCAM number counts; the upper limit 'CAT' is from Renault et al. (2001) and the cross upper limits W/B are from Biller et al. (1998). At longer wavelength, we have the 60 μm estimate from Miville-Deschênes et al. (2002) (△), the upper limit from Finkbeiner, Davis & Schlegel (2000), and the lower limit from number counts at 60 μm (Lonsdale et al. 1990); at 140 and 240 μm are displayed the Lagache et al. 2000 (⋄) and Hauser et al. (1998) (⋆) DIRBE values; at 100 μm is given the lower limit from Dwek et al. (1998) together with the estimates from Renault et al. (2001) (+) and the determination of Lagache et al. (2000) (⋄); at 170 μm (Puget et al. 1999) and 850 μm (Barger et al. 1999) are lower limits from number counts. The analytic form of the CIB at the *FIRAS* wavelengths is from Fixsen et al. (1998). The CIB derived from the model at selected wavelengths is given by filled squares.

Table 2. Comparison of the predicted CIB fluctuations (for $S < S_{\rm max}$ in Jy^{-2} sr^{-1}) and the observations.

λ (μm)	$S_{\rm max}$ (mJy)	Observations (Jy^{-2} sr^{-1})	References	Model (Jy^2 sr^{-1})
170	1000	$\sim$25 000	Sorel et al. (in preparation)	23 694
170	250	13 000 $\pm$ 3000	Matsuhara et al. (2000)	15 644
170	100	7400	Lagache et al. (2000)	11 629
100	700[a]	5800 $\pm$ 1000	Miville-Deschênes et al. (2002)	10 307
90	150	12 000 $\pm$ 2000	Matsuhara et al. (2000)	5290
60	1000	1600 $\pm$ 300	Miville-Deschênes et al. (2002)	2507

[a]Bright sources in Miville-Deschênes et al. (2002) are removed at 60 and 100 μm using the cut of 1 Jy at 60 μm. Since the 60-μm sources are mostly starburst galaxies, we estimate that 1 Jy at 60 μm is equivalent to 0.7 Jy at 100 μm.

brightest sources that make up the bulk of the fluctuations (sources with fluxes $S > S_{\rm max}$). When $S_{\rm max}$ is quite high (of the order of 500 mJy–2 Jy), the fluctuations are dominated by the strongest sources, making the result very dependent on the accuracy of the evaluation of $S_{\rm max}$. This is why the comparison between observations and model is very difficult.[4] For $S_{\rm max}$ around 50–150 mJy, the fluctuations are dominated by the faint and numerous sources that dominate the CIB and the values do not depend critically on the exact value of $S_{\rm max}$. We see from Table 2 that, although for some observations the model can be lower or greater by a factor 1.5 in amplitude, we have an overall very good agreement. We stress that reproducing the CIB fluctuations gives strong constraints on the LF evolution. For example, evolution such that we better reproduce the 850-μm counts gives too high CIB fluctuations. Future observations with better accuracy will show if these minor discrepancies disappear or are indicative that the bright submillimetre counts are overestimated as a result of a high fraction of gravitationally lensed sources (Perrotta et al. 2002), or are simply indicative that the present phenomenological model is too simple! The level of the predicted CIB fluctuations for dedicated experiments (as for example *Boomerang* or *Maxima*), with respect to the cirrus confusion noise and instrumental noise will be discussed in detail in Piat et al. (in preparation).

At 170 μm, it is clear from Fig. 12 that the redshift distributions of sources that make up the CIB and those making up the bulk of the fluctuations are similar. The fluctuations are not dominated by bright sources just below the detection threshold but by numerous sources at higher redshift. Thus, in this case, studying the CIB fluctuations gives strong constraints on the CIB source population. This is true in the whole submillimetre–millimetre range. The population of galaxies where the CIB peaks will not be accessible by direct detection in the coming years. For example, *SIRTF* will resolve about 20 per cent of the background at 160 μm (Dole, Lagache & Puget 2002), PACS about 50 per cent at 170 μm (Section 7.2.2) and SPIRE less than 10 per cent at 350 μm (Section 7.2.1).

In conclusion, we have seen that our model gives number counts, redshift distributions, CIB intensity and fluctuations that reproduce all the present observations. It can now be used for predictions about future experiments, in particular for *Herschel*, *Planck* and ALMA observations. For *SIRTF*, a complete and more detailed study, including simulations and a detailed discussion on the confusion, can be found in Dole et al. (2002).

[4] We cannot compare the model predictions with the Kiss et al. (2001) results since we have no information on $S_{\rm max}$.

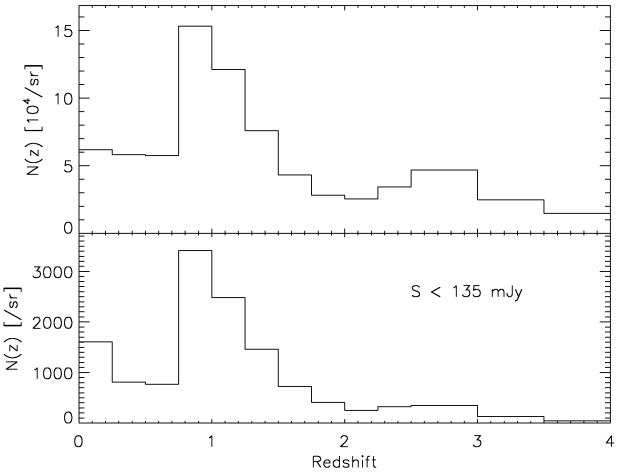

Figure 12. Redshift distribution of sources making up the CIB intensity and its fluctuations ($S < 135$ mJy) at 170 μm.

7 PREDICTIONS FOR FUTURE EXPERIMENTS

7.1 The confusion noise from extragalactic sources

The confusion noise[5] is usually defined as the fluctuations of the background sky brightness below which sources cannot be detected individually. These fluctuations are caused by intrinsically discrete extragalactic sources. In the far-IR, submillimetre and millimetre wavelengths, as a result of the limited size of the telescopes compared to the wavelength, confusion noise plays an important role in the total noise budget. In fact, confusion noise is often greater than instrumental noise, and thus severely limits the survey depth. The total variance σ^2 of a measurement within a beam due to extragalactic sources with fluxes less than $S_{\rm lim}$ is given by

$$\sigma^2 = \int f^2(\theta,\phi)\,{\rm d}\theta\,{\rm d}\phi \int_0^{S_{\rm lim}} S^2\,\frac{{\rm d}N}{{\rm d}S}\,{\rm d}S, \qquad (12)$$

where $f(\theta,\phi)$ is the two-dimensional beam profile (sr), S the flux (Jy) and ${\rm d}N/{\rm d}S$ the differential number counts (Jy^{-1} sr^{-1}). We call $S_{\rm lim}$ the confusion limit.

[5] We only consider the confusion noise due to extragalactic sources since, in the high galactic latitude cosmological fields, the cirrus confusion noise is negligible.

The confusion noise can be determined using two criteria: the so-called photometric and source density criteria (see Dole et al. 2002 , for a full description). The photometric criterion is related to the quality of the photometry of detected sources, the flux measured near $S_{\rm lim}$ being severely affected by the presence of fainter sources in the beam. It is defined by the implicit equation

$$S_{\rm lim} = q_{\rm phot}\,\sigma(S_{\rm lim}) \tag{13}$$

where $q_{\rm phot}$ measures the photometric accuracy and is usually taken between 3 and 5.

The source density criterion is related to the completeness of detected sources above $S_{\rm lim}$ directly related to the probability to lose sources too close to each other to be separated. There is a threshold above which the density of sources above $S_{\rm lim}$ is such that a significant fraction of the sources is lost (it is impossible to separate the individual sources any more). For a given source density (with a Poissonian distribution) $N(>S)$, corresponding to a flux limit $S_{\rm lim}$, the probability P to have the nearest source with flux greater than $S_{\rm lim}$ located closer than the distance $\theta_{\rm min}$ is

$$P(<\theta_{\rm min}) = 1 - \exp\left(-\pi N \theta_{\rm min}^2\right), \tag{14}$$

where $\theta_{\rm min}$ is the distance below which sources cannot be separated and is a function of the beam profile. If we use $\theta_{\rm FW}$ to denote the full width at half-maximum (FWHM) of the beam profile, $\theta_{\rm min}$ can conveniently be expressed in terms of $\theta_{\rm FW}$, $\theta_{\rm min} = k\theta_{\rm FW}$. As an illustration, simulations of source extraction at the *MIPS/SIRTF* wavelengths show that $k = 0.8$ should be achievable (Dole et al. 2002). Therefore, in the following, we fix $k = 0.8$. We choose the maximum acceptable probability of not being able to separate the nearest source $P_{\rm max} = 0.1$. In this case, the source density is equal to $1/17.3\Omega$ (Table 3) and the corresponding most probable distance is about $1.7\theta_{\rm FW}$. Using equation (14), we can derive $N(>S)$ and thus find the corresponding $S_{\rm lim}$. Then, using equation (12), we compute σ. The source density criterion leads to an equivalent value $q_{\rm density} = S_{\rm lim}/\sigma$. If $q_{\rm density}$ is greater than standard values of $q_{\rm phot}$ (3 to 5), then the confusion noise is given by the source density criterion. If not, then the photometric criterion has to be used to derive the confusion noise. The classical confusion limit of one source per 30 beams corresponds to $k = 1$ and $P \sim 0.1$. Nevertheless it can still lead to mediocre photometry for very steep log N–log S.

The transition between the photometric and source density criterion is around 200 μm, depending on telescope diameters. For example, for *SIRTF*, at 24 and 70 μm, the source density criterion gives $q_{\rm density} \sim 7$ (Dole et al. 2002). In this case, the source density criterion has to be used to derive the source confusion and it leads to a very good photometric quality. On the contrary, at the *Planck* wavelengths, the source density criterion gives $q_{\rm density} \sim 1$, leading to source detection limited by the photometric quality. Furthermore, this illustrates the limits of doing high signal-to-noise ratio observations 'to beat the confusion'.

In the following, we derive the confusion noise for future long-wavelength dedicated surveys. We assume that the sources are randomly distributed on the sky. The effect of the clustering on the confusion noise will be investigated by Blaizot et al. (in preparation) using the hybrid model described in Guiderdoni et al. (2001) and Hatton et al. (2002). The number counts at long wavelengths derived from the model and useful for the following predictions are shown in Fig. 13.

Table 3. Number of beams per source for different probability P to have the nearest source located closer than the distance $\theta_{\rm min} = k\theta_{\rm FW}$ with $\theta^2_{\rm FW} \sim \Omega/1.1$ (valid for both Gaussian and Airy disc beams).

	$P = 0.05$	$P = 0.1$	$P = 0.15$
$k = 0.8$	35.6	17.3	11.2
$k = 0.9$	45.1	22.0	14.2
$k = 1.0$	55.7	27.1	17.6

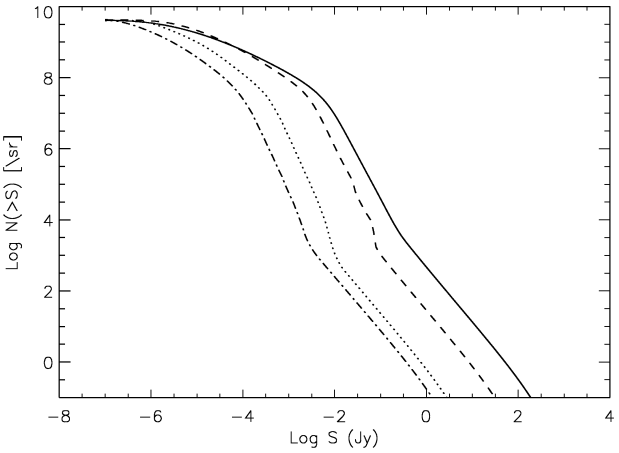

Figure 13. Predicted number counts at 350 μm (full line), 550 μm (dashed line), 1300 μm (dotted line) and 2097 μm (dot-dashed line).

7.2 The *Herschel* deep surveys

The *Herschel Space Observatory* (Pilbratt 2001) is the fourth cornerstone mission in the European Space Agency science programme. It will perform imaging photometry and spectroscopy in the far-IR and submillimetre parts of the spectrum, covering approximately the 60–670 μm range. *Herschel* will carry a 3.5-m diameter passively cooled telescope. Three instruments share the focal plane: two cameras/medium-resolution spectrometers, PACS and SPIRE, and a very high-resolution heterodyne spectrometer, HIFI.

In Table 4 are shown the confusion noises and limits at PACS and SPIRE wavelengths using the photometric and source density criteria. At the PACS wavelengths, the source density criterion leads to confusion limits 2–6 times higher than the photometric criterion with $q_{\rm phot} = 5$. For SPIRE, at 250 μm, the limits obtained using

Table 4. PACS and SPIRE 1σ confusion noise and its associated flux limit ($S_{\rm lim}$) for the photometric criterion ($q_{\rm phot} = 5$) and the source density criterion (with the equivalent $q_{\rm density}$).

		σ (mJy)	$S_{\rm lim}$ (mJy)
PACS 75 μm	$q_{\rm phot} = 5.0$	2.26×10^{-3}	1.12×10^{-2}
	$q_{\rm density} = 8.9$	1.42×10^{-2}	1.26×10^{-1}
PACS 110 μm	$q_{\rm phot} = 5.0$	1.98×10^{-2}	1.0×10^{-1}
	$q_{\rm density} = 8.7$	1.02×10^{-1}	8.91×10^{-1}
PACS 170 μm	$q_{\rm phot} = 5.0$	3.97×10^{-1}	2.00
	$q_{\rm density} = 7.13$	9.93×10^{-1}	7.08
SPIRE 250 μm	$q_{\rm phot} = 5.0$	2.51	12.6
	$q_{\rm density} = 5.2$	2.70	14.1
SPIRE 350 μm	$q_{\rm phot} = 5.0$	4.4	22.4
	$q_{\rm density} = 3.6$	3.52	12.6
SPIRE 550 μm	$q_{\rm phot} = 5.0$	3.69	17.8
	$q_{\rm density} = 2.5$	3.18	7.94

Table 5. Designed surveys that could be done with SPIRE (numbers are from the 350-μm channel).

Surface (deg^2)	$5\sigma_{inst}$ (mJy)	$5\sigma_{conf}$ (mJy)	$5\sigma_{tot}$ (mJy)	Days	Number of sources	Per cent resolved CIB
400	100	28.2[a]	103.9	18	4768	1.0
100	15.3	22.4	27.1	90	33 451	6.7
8	7.5	22.4	23.6	64	3533	7.8

[a]Unresolved sources below $5\sigma_{inst} = 100$ mJy induce a confusion noise of $\sigma_{conf} = 5.63$ mJy.

the two criteria are very close and then, at longer wavelengths, the photometric quality constrains the confusion limit.

Extragalactic surveys will be conducted by both the PACS and SPIRE instruments. Up to now, the trade-off between large-area, shallow versus small-area, deep/ultradeep observations has not been finalized. In the following two sections are examples of extragalactic surveys that could be done.

7.2.1 The SPIRE surveys

For large-area scan-mapping observations, the current estimates of time needed to map 1 deg^2 to an instrumental noise level of 3 mJy ($1\sigma_{inst}$) is about 1.7, 2 and 2.1 d at 250, 350 and 550 μm respectively (Matt Griffin, private communication). Three kinds of surveys could be done with SPIRE (Table 5):

(i) A very large area (two approximately 14×14 deg^2, i.e. ∼400 deg^2) survey at the noise level of $5\sigma_{inst} = 100$ mJy at 350 μm (92 mJy at 250 μm and 102 mJy at 550 μm).

(ii) A confusion-limited survey of about 100 deg^2. To reach a $5\sigma_{inst}$ noise limit of 14.1, 22.4 and 17.8 mJy, one needs 192, 90 and 149 d at 250, 350 and 550 μm, respectively.

(iii) A very deep survey, down to the confusion limit, to extract as much information as possible about the underlying population. For example, mapping 8 deg^2 to $5\sigma_{inst} = 7.5$ mJy at 350 μm would take 64 d.

We concentrate, in the following, on the 350-μm band (although SPIRE observes the three bands simultaneously). The number of detected sources for each survey is given in Table 5 and the redshift distribution in Fig. 14.

7.2.1.1. The very large area survey This survey is well suited to the *Planck* sensitivity (see Table 7). It would provide better positions for the *Planck* point sources and the combination with the *Planck* data would improve the spectral and spatial characterization of foregrounds. It will take about 18 d, which is a small amount of time compared to the enormous progress it would bring for the component separation problem for all observations in this wavelength range. The very large area survey will detect mostly nearby sources but hundreds of objects could be detected at $z > 1$. It will also explore the cirrus component. Moreover, thanks to its surface coverage, this survey will detect the rare and high-z objects about which little is known today.

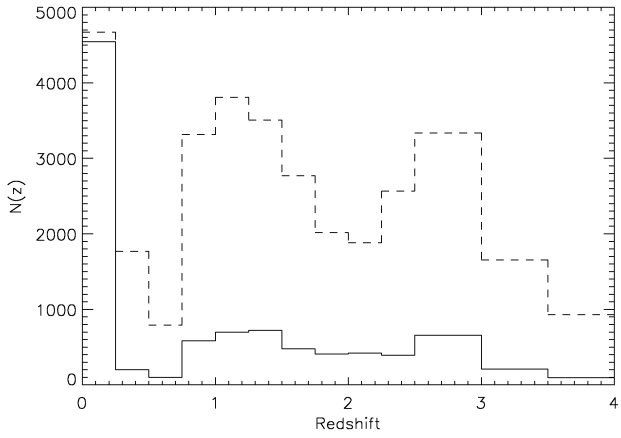

Figure 14. SPIRE 350 μm redshift distribution for sources detected in the very large area survey (full line, $S > 103.9$ mJy, multiplied by 2) and the confusion-limited survey (dashed line, $S > 27.1$ mJy).

7.2.1.2. The confusion-limited survey For the confusion-limited survey, there are mainly two peaks in the redshift distribution: one at $z \sim 0$ due to the cold sources, and the other between 0.8 and 3 due to the starburst galaxies. The number of starburst galaxies detected between 0.8 and 3 does not vary much. Fig. 15 predicts the number of starburst galaxies that the confusion-limited survey will detect at 350 μm per log interval of luminosity (this figure does not include the cold population, which contributes mostly locally). The evolution of the 10^{12}–10^{13} $L_\odot$ galaxies will be measured from $z \sim 0.5$ to 2.5. Galaxies with $L \sim 3 \times 10^{11}$ $L_\odot$ will only be accessible at $z \sim 0.1$. The nature and number of the highest-luminosity objects are important to test cosmological theories, and thus populating the high-redshift bins with enough objects to ensure <14 per cent Poisson noise (corresponding to 50 sources) is a critical driver for the size of the sample, and, accordingly, the area required for the survey. Based on our model, we see from Fig. 15 that, to meet this ∼14 per cent goal for galaxies in the range 10^{12}–10^{13} $L_\odot$ at $z < 2.5$, an area of 100 deg^2 is the minimum required.

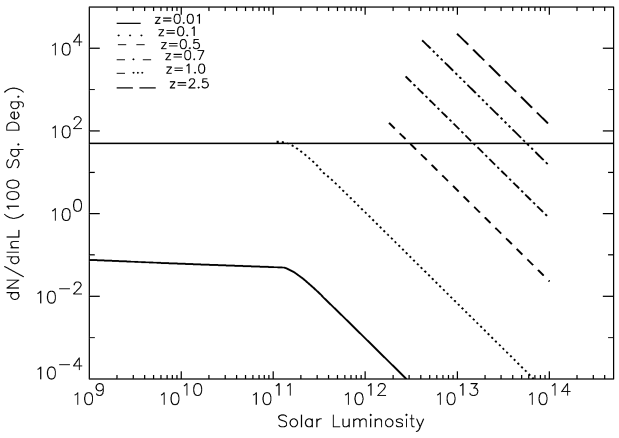

Figure 15. Number of starburst galaxies that can be detected in different redshift ranges (with a $\Delta z/z = 0.5$) at 350 μm by the confusion-limited survey of 100 deg^2 as a function of bolometric luminosity. The horizontal line shows the 50 sources needed in a $\Delta z/z = 0.5$ bin for ∼14 per cent accuracy. The plots are limited to the fluxes above the detection limit and to luminosities below 10^{14} $L_\odot$.

7.2.1.3. The very deep survey The confusion-limited surveys will detect only ∼7 per cent of the CIB (1 per cent for the very large area survey). In this case, studying the fluctuations will provide information on the underlying source population. The redshift distribution of sources making up the bulk of the CIB and the fluctuations at 350 μm are very similar. Thus, the fluctuations will be a unique opportunity to obtain information, in particular, on sources that dominate the CIB (sources with $L \sim 3 \times 10^{11}$ $L_{\odot}$), at redshifts where they cannot be detected individually. To detect and study them, a field with high signal-to-noise ratio is needed. Moreover, the size of the field should be large enough to try to detect the source clustering and not only be limited to the Poissonian noise detection (which is about 4300 Jy^2 sr^{-1}). Since source clustering is expected at scales between 1 and 5 deg (Knox et al. 2001), a field of about 8 deg^2 is the minimum required. This field could be part of the confusion-limited survey, which will certainly be split into several smaller area surveys.

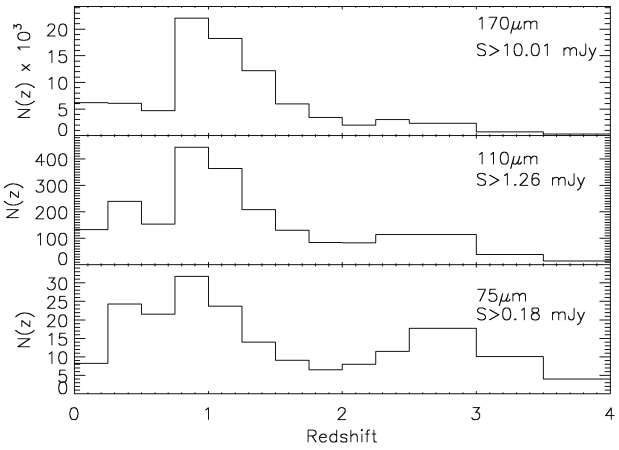

Figure 16. From bottom to top: redshift distribution for the ultradeep, deep and shallow PACS surveys at 75, 110 and 170 μm respectively.

7.2.2 The PACS surveys

For the whole field of view of ∼1.75 × 3.5 $arcmin^2$, the current estimates of time needed to reach $5\sigma_{\rm inst} = 3$ mJy is 1 h (Albrecht Poglitsch, private communication). At 75, 110 and 170 μm, the confusion limits are about 0.13, 0.89 and 7.08 mJy, with $q_{\rm density}$ of 8.9, 8.7 and 7.1, respectively. To reach the confusion limit for one field of view, i.e. $5\sigma_{\rm inst} = 0.1$, 0.9 and 7.1, we need 567, 11 and 0.18 h at 75, 110 and 170 μm, respectively. Since for PACS the confusion limits and the time to reach those sensitivities are very different at the three wavelengths, three kinds of surveys could be done, which, schematically, will probe the CIB in three bands:

(i) A shallow survey of 20 deg^2 down to the confusion limit at 170 μm. This survey is dedicated to probe the CIB at 170 μm and to study the correlations. Such a survey will take 88 d.

(ii) A deep survey down to the confusion limit at 110 μm. A good compromise between the covered surface and the time needed is a field of 25 × 25 $arcmin^2$, which will take about 67 d.

(iii) An ultradeep survey down to the confusion limit at 75 μm (or a little bit below the confusion limit). To map a 5 × 5 $arcmin^2$ field, 96 d are needed.

These three surveys correspond to about the same amount of time as the SPIRE surveys. Obviously, the PACS surveys have to be done within the same areas as the SPIRE ones.

PACS observes simultaneously the 170 and 110 μm channels or the 170 and 75 μm channels. Ideally a combination 75/110 μm and 75/170 μm would have been preferable, since the 170-μm observation in the deep and ultradeep surveys will not bring new science compared to the large area survey. On the contrary, observing the shortest wavelengths in the shallow survey will detect the very luminous, hot and rare galaxies that may be missed in the deep and ultradeep surveys.

The three surveys will detect thousands of sources at $z \sim 1$ (Fig. 16) and will probe most of the CIB source population (they will resolve about 49, 77 and 87 per cent of the CIB at 170, 110 and 75 μm respectively; Table 6).

At 170 μm, the shallow survey will give an unprecedented measurement of the evolution of the 10^{11}–10^{12} $L_{\odot}$ galaxies from $z \sim$ 0.25 to 1 and the evolution of the 10^{12}–10^{13} $L_{\odot}$ galaxies from $z \sim$ 0.5 to 3 (with enough objects to ensure <10 per cent Poisson noise). Since half of the background is resolved into discrete sources at 170 μm, one complementary approach is to reduce the surface of the shallow survey to have a better signal-to-noise ratio and thus study the underlying population. However, to study the correlation in the IR background, a minimum of 8 deg^2 is required. A survey at $S_{\rm min} =$ 8 mJy, corresponding to $5\sigma_{\rm inst} = 3.7$ mJy, would take around 128 d for 8 deg^2. Such a survey would give less statistics for the resolved sources but would help in understanding the whole CIB population. With an 8 deg^2 field, the measurement of high-luminosity source evolution would still be possible with a high degree of accuracy.

In conclusion, PACS will resolve about 80 per cent of the CIB around 100 μm (*SIRTF* will resolve at most around 55 per cent of the CIB at 70 μm and 20 per cent at 160 μm; Dole et al. 2002). It will definitely resolve the question of the population making up the CIB near its emission peak. It will measure with unprecedented accuracy the history of the IR-traced star formation up to $z \sim 1.5$. For higher redshifts, information will come mainly from the SPIRE surveys. Although SPIRE will resolve less than 10 per cent of the CIB in the submillimetre, it will provide unprecedented information

Table 6. Designed surveys that could be done with PACS.

Surface	λ (μm)	Days[a]	$5\sigma_{\rm inst}$ (mJy)	$S_{\rm min}$[b] (mJy)	Number of sources	Per cent resolved CIB
20 deg^2	170	88	7.08	10.01	87 322	48.7
625 $arcmin^2$	110	67	0.89	1.26	1955	77
25 $arcmin^2$	75	96	0.13	0.18	192	87

[a] Depending on the scanning/chopping/beam switching strategy, there may be some overhead of about 20 per cent.

[b] $S_{\rm min} = \sqrt{(5\sigma_{\rm inst})^2 + S_{\rm lim}^2} = \sqrt{2} \times S_{\rm lim}$.

Table 7. *Planck* sensitivities ($5\sigma_{\rm inst}$), confusion limit ($S_{\rm lim} = 5\sigma_{\rm conf}$), confusion induced by sources between $S_{\rm lim}$ and $5\sigma_{\rm inst}$ ($5\sigma_{\rm add}$), and total 5σ noise (which is the quadratic sum of the contribution from the detector noise and the extragalactic confusion noise). Also given are the cold, starburst and total galaxy densities.

λ (μm)	$5\sigma_{\rm inst}$ (mJy)	$5\sigma_{\rm conf}$ (mJy)	$5\sigma_{\rm add}$ (mJy)	$5\sigma_{\rm tot}$ (mJy)	$N_{\rm cold}(S > 5\sigma_{\rm tot})$ ($\rm sr^{-1}$)	$N_{\rm SB}(S > 5\sigma_{\rm tot})$ ($\rm sr^{-1}$)	$N(S > 5\sigma_{\rm tot})$ ($\rm sr^{-1}$)
350	216.5	447	0	497	1342	40	1382
550	219	200	7.9	297	187	15	202
850	97	79.4	3.2	125	72	8	80
1380	57.5	22.4	2.6	62	35	4	39
2097	41.5	11.2	2.4	43	23	3	26

on the evolution of galaxies up to $z \sim 3$ and also on the underlying population, which will be very hard to detect from the ground due to the small area of the present surveys.

7.3 The *Planck* all-sky survey

For the *Planck* wavelengths, the confusion limits are given by the photometric criterion.[6] With $q_{\rm phot} = 5$, they are about 447, 200, 79.4, 22.4 and 11.2 mJy at 350, 550, 850, 1380 and 2097 μm respectively (for detection only, $q_{\rm phot} = 3$ is better and leads to the following confusion limits: 251, 112, 44.7, 14.1 and 6.31 at 350, 550, 850, 1380 and 2097 μm respectively). The confusion limit (with $q_{\rm phot} = 5$) is above the 5σ instrumental noise at 350 μm, comparable at 550 μm and then below at longer wavelengths. It can be compared to the values given in table 2.1 of the *HFI Proposal for the Planck Mission* (1998). In that table, the confusion limits have been computed using Ω rather than $\int f^2(\theta, \phi)\, {\rm d}\theta\, {\rm d}\phi$ in equation (12). This leads to a systematic overestimate of $\sigma_{\rm conf}$ by a factor of 1.33. Correcting for this factor, the ratio of those estimates to the present ones increases from 350 to 2097 μm from 1.2 to 3.

To compute the number of sources expected in the *Planck* survey, we use a cut in flux equal to $5\sigma_{\rm tot}$ such as

$$\sigma_{\rm tot} = \sqrt{\sigma_{\rm inst}^2 + \sigma_{\rm conf}^2 + \sigma_{\rm add}^2}, \tag{15}$$

where $\sigma_{\rm conf}$ for *Planck* is given by $\sigma_{\rm conf} = S_{\rm lim}/5$. $\sigma_{\rm add}$ is an additional noise due to unresolved sources with fluxes between $S_{\rm lim}$ and $5\sigma_{\rm inst}$:

$$\sigma_{\rm add}^2 = \int f^2(\theta, \phi)\, {\rm d}\theta\, {\rm d}\phi \int_{S_{\rm lim}}^{5\sigma_{\rm inst}} S^2 \frac{{\rm d}N}{{\rm d}S}\, {\rm d}S. \tag{16}$$

This additional term is only present when $5\sigma_{\rm inst}$ is greater than the confusion limit (as for example for the SPIRE very large survey).

Final sensitivities on point sources, together with the number of detected sources for *Planck*, are given in Table 7. At all wavelengths, the sensitivity of the survey is in the Euclidean part of the number counts. *Planck* will not be able to constrain, with the resolved sources, the evolution of the submillimetre galaxies but it will give an absolute calibration of the bright number counts, which will not be provided by any other planned instruments. Moreover, by covering the whole sky, it will probably detect the most spectacular dusty object of the observable Universe, such as hyperluminous or strongly lensed starburst or AGN galaxies, as well as extreme sources not included in the model.

Note, however, that the sensitivities have been computed with an instrumental noise derived from a mean integration time. With the *Planck* scanning strategy, some high-latitude regions (where cirrus contamination is low) will be surveyed more deeply, leading to an instrumental noise about three times lower. In such high-redundancy parts of the sky, the *Planck* survey will be limited by the confusion noise (except at 2097 μm, where the instrumental noise and confusion noise are of the same order). In those regions, *Planck* will produce unique maps of the CIB fluctuations. CIB anisotropies are mainly contributed by moderate- to high-redshift star-forming galaxies, whose clustering properties and evolutionary histories are currently unknown. *Planck* observations will thus complement the future far-IR and submillimetre telescopes from ground and space that will perform deep surveys over small areas. These surveys will resolve a substantial fraction of the CIB but will probably not investigate the clustering of the submillimetre galaxies since it requires surveys over much larger areas.

7.4 Requirements for future experiments for very large deep surveys in the infrared/submillimetre/millimetre domain

Since (1) the far-IR and submillimetre sources are often associated with mergers or interacting galaxies and (2) their energy output is dominated by high-luminosity sources at high redshift [which might be related to the optical where the output is dominated by high-brightness sources at high redshift (Lanzetta et al. 2002)], they have to be studied in detail in the long-wavelength range and at high redshift ($z \geqslant 3$) as a tool to understand the merging process and the physics of the first non-linear structures.

Two kinds of requirements have to be met by the post-*SIRTF*, *Herschel* and *Planck*, surveys:

(i) They have to find the interesting high-redshift sources, which are early mergers made up of building blocks not yet much affected by star formation and evolution. The number of such sources have to be large enough to do statistical studies.

(ii) Once these sources are found, future experiments have to have enough sensitivity and angular resolution to study them in detail.

To quantify the first requirement, we compute the surface needed to detect more than 100 sources with luminosities of 3×10^{11} and 3×10^{12} $\rm L_\odot$ in each redshift range (Table 8). At high redshift, we need surveys of about a 100 $\rm deg^2$ to find enough high-luminosity objects to do statistical studies. If enough area is covered, we need moreover a high sensitivity; for example, we have to reach 0.21 mJy at 850 μm for $L = 3 \times 10^{11}$ $\rm L_\odot$ galaxies (dominating the LF at $z \sim 1$) and 1.9 mJy at 850 μm (or 0.9 mJy at 1300 μm) for $L = 3 \times 10^{12}$ $\rm L_\odot$ galaxies (dominating the LF at $z > 2$). The fluxes of typical 3×10^{12} $\rm L_\odot$ galaxies at high-z are just, for single-antenna telescopes, at the confusion limit. With the future wide-field imaging instruments on these telescopes, for example SCUBA-2 (Holland

[6] The density criterion leads to $q_{\rm density}$ from 1.5 to 0.8 from 350 to 2097 μm respectively.

Table 8. Sky area in square degrees to be covered to detect more than 100 sources in a redshift range $\Delta z/z = 0.3$, for 3×10^{11} $L_\odot$ (top) and 3×10^{12} $L_\odot$ (bottom) starburst galaxies.

z	S_{350} (mJy)	S_{850} (mJy)	S_{1300} (mJy)	Surface
3×10^{11} $L_\odot$				
1	2.95	0.30	0.09	0.7
3	0.78	0.25	0.08	1.8
5	0.21	0.26	0.11	10
7	0.065	0.21	0.12	60
3×10^{12} $L_\odot$				
1	22.1	2.05	0.7	5.7
3	7.51	1.82	0.6	6.1
5	2.73	2.07	0.8	53
7	1.01	1.89	0.9	398

et al. 2001) and BOLOCAM (Glenn et al. 1998), 100 deg^2 at the 1 mJy level at 1300 μm could be mapped in a reasonable amount of time. However, with a 10/15 arcsec beam, it will be very difficult to make optical identifications and follow-up observations at other wavelengths.

To reach the sensitivity of the 3×10^{11} $L_\odot$ galaxies at high z, we need to have a very good angular resolution not limited by confusion. Table 9 gives the angular resolution together with the telescope diameter needed to reach 10, 30, 60 and 80 per cent of the CIB at 350, 850 and 1300 μm. To resolve 80 per cent of the background at 1300 μm, we need a telescope diameter of about 173 m (!) and a diameter of about 113 m (!) at 850 μm and 23 m at 350 μm. In conclusion, finding objects that make up the bulk of the CIB at long wavelengths will be a very challenging task! This leaves an open question: How can we find these objects? In the mid-IR, the *Next Generation Space Telescope* (*NGST*) will be a great tool. However, *NGST* observations will have two limitations: (1) the redshift up to which the dust component can be observed is limited to 4–5; and (2) the stellar component can be observed at higher z but the experience of combined optical/near-IR and far-IR observations shows how difficult it is to identify the galaxies that have most of their output energy in the far-IR from optical and near-IR data alone. Therefore, the alternative today is to make interferometers efficient enough to carry out large surveys.

For the second requirement, i.e. study in detail the physics of the objects, observations have to have enough sensitivity to observe the subcomponents of merging objects at high z (a 3×10^{10} $L_\odot$ subcomponent at $z = 5$ has a flux of about 0.014 mJy at 350 μm and of about 0.028 mJy at 850 μm). Moreover, an angular resolution of about 0.2–1 arcsec together with spectroscopic capabilities are needed. For that, the submillimetre and millimetre interferometers are the only tools, as shown by the recent spectacular observations of a high-redshift quasar with the IRAM interferometer (Cox et al. 2002). Lower-luminosity sources will require the ALMA[7] or SPECS/SPIRIT (Leisawitz et al. 2001) interferometers.

Table 9. Angular resolution and telescope diameter needed to have the confusion limit at a flux level $S_{\rm min}$ such that sources above $S_{\rm min}$ contribute about 10, 30, 60 and 80 per cent of the CIB (top: 350 μm; middle: 850 μm; bottom: 1300 μm).

Per cent CIB	S_{350} (mJy)	log N (sr^{-1})	θ^a (arcsec)	D^b (m)
80	0.9	8.01	3.2	23
60	2.5	7.71	4.8	15.1
30	8	7.09	10	7.2
10	18	6.32	23.7	3.0
Per cent CIB	S_{850} (mJy)	log N (sr^{-1})	θ^a (arcsec)	D^b (m)
80	0.05	8.35	1.6	113
60	0.2	8.03	3.0	59
30	1	7.45	7.0	25
10	2	6.77	15.3	12
Per cent CIB	S_{1300} (mJy)	log N (sr^{-1})	θ^a (arcsec)	D^b (m)
80	0.02	8.38	1.6	173
60	0.06	8.10	2.7	101
30	0.3	7.48	6.6	40
10	0.7	6.75	15.6	17

[a] θ has been computed using $N\theta^2 = 1/30$.
[b] $D = \lambda/\theta$.

7.5 The case of ALMA

Thanks to the negative k-correction, high-redshift sources are accessible from the ground at submillimetre and millimetre wavelengths. ALMA, a synthesis radio telescope (about 64 telescopes of 12-m diameter) that will operate at submillimetre and millimetre wavelengths, will image the Universe with unprecedented sensitivity and angular resolution from the high-altitude Llano de Chajnantor, in northern Chile. It will be one of the largest ground-based astronomy projects of the next decade after VLT/VLTI, and, together with the *NGST*, one of the two major new facilities for world astronomy coming into operation by the end of the next decade. ALMA, with its angular resolution, great sensitivity and spectroscopic capabilities, will reveal in detail, in the high-z galaxies, the astrophysical processes at work. Moreover, ALMA will be free of limitations due to source confusion and will therefore allow very faint galaxies to be detected. In this section, we discuss mostly the abilities of ALMA to find large enough samples of high-redshift sources to do statistical studies and probe the CIB source population. Of course ALMA will also be used to study their structure and physics.

At 1300 μm, to find enough $\sim 3 \times 10^{11}$ $L_\odot$ high-z sources, we need to cover a surface of at least 5 deg^2 at a 5σ level of about 0.1 mJy (Table 8). Such a survey will resolve about 50 per cent of the CIB. To resolve ~80 per cent of the CIB, one needs to reach a 5σ level of about 0.02 mJy (Table 9). Therefore two kinds of surveys could be considered: a large-area (~5 deg^2) and an ultradeep (~10 arcmin^2) survey. For both surveys, the compact configuration has enough resolution not to be limited by the confusion. At 1300 μm, a 5σ detection of 2.3 mJy is reached in 1 s for a beam area of 0.16 arcmin^2 [see *ALMA Proposal for Phase 2* and Blain (2001)]. For the two types of surveys this gives the following.

(i) The large area survey: 5 deg^2, $5\sigma_{1300} = 0.1$ mJy (50 per cent of the CIB). A 1 deg^2 field requires 22 500 pointings, each with 529 s of observations, for a total of 138 d. For 5 deg^2, 690 d are needed, i.e. 1.9 yr.

(ii) The ultra-deep survey: 10 arcmin^2, $5\sigma_{1300} = 0.02$ mJy (80 per cent of the CIB). A 10 arcmin^2 field requires 625 pointings, each with 13 225 s of integration, for a total of 96 d.

In conclusion, if we want to achieve the two goals, namely (i) detect enough early mergers made up of building blocks not yet much affected by star formation and evolution, and (ii) probe most of the CIB source population at large wavelengths, we will have to

[7] http://www.eso.org/projects/alma/, http://www.mma.nrao.edu/

do extragalactic surveys with ALMA using a substantial fraction of the time to find the sources. Such large surveys including the whole ALMA collaboration would be much more efficient in terms of scientific progress than smaller area surveys conducted by individual smaller teams.

8 SUMMARY

We have developed a phenomenological model that constrains in a simple way the IR luminosity function evolution with redshift, and fits all the existing source counts and redshift distribution, CIB intensity and, for the first time, CIB fluctuation observations from the mid-IR to the submillimetre range. The model has been used to make some predictions for future *Herschel* deep survey observations and the all-sky *Planck* survey. It comes out that the planned experiments (*SIRTF*, *Herschel*, *Planck*) will be mostly limited by the confusion. To find a large number of objects that dominate the LF at high redshift ($z > 2$), future experiments need both angular resolution and sensitivity. This can be achieved in the submillimetre only through use of interferometers such as ALMA. However, mapping large fractions of the sky with high signal-to-noise ratio will take a lot of time (for example, 1.9 yr to map 5 deg^2, which resolve 50 per cent of the CIB at 1.3 mm with ALMA).

ACKNOWLEDGMENTS

HD thanks the MIPS project (under NASA Jet Propulsion Laboratory subcontract #P435236) for support during part of this work and the Programme National de Cosmologie and the Institut d'Astrophysique Spatiale for some travel funding.

REFERENCES

Almaini O., Lawrence A., Boyle B. J., 1999, MNRAS, 305, 59
Altieri B., Metcalfe L., Kneib J. P. et al., 1999, A&A, 343, L65
Aussel H., Cesarsky C. J., Elbaz D., Stark J. L., 1999, A&A, 342, 313
Balland C., Devriendt J. E. G., Silk J., 2002, MNRAS, submitted (astro-ph/0210030)
Barger A. J., Cowie L. L., Sanders D. B., 1999, ApJ, 518, L5
Barger A. J., Cowie L. L., Mushotzky R. F., Richards E. A., 2001, AJ, 121, 662
Bertin E., Dennefeld M., Moshir M., 1997, A&A, 323, 685
Bertoldi F., Menten K. M., Kreysa E., Carilli C. L., Owen F., 2000, in Wilner D. J., ed., Proc. 24th Meeting of the IAU, Highlights of Astronomy Vol. 12, Cold Gas and Dust at High Redshift. Astron. Soc. Pac., San Francisco, in press (astro-ph/0010553)
Biller S. D., Buckley J., Burdett A. et al., 1998, Phys. Rev. Lett., 80, 2992
Biviano A., Metcalfe L., Altieri B., 2000, in Mazure A., Le Fevre O., Le Brun V., eds, ASP Conf. Ser. Vol. 200, 1999 Marseille IGRAP Conf., Clustering at High Redshifts. Astron. Soc. Pac., San Francisco, p. 101
Blain A. W., 2001, in Wootten A., ed., ASP Conf. Ser. Vol. 235, Science with the Atacama Large Millimeter Array. Astron. Soc. Pac., San Francisco, p. 261 (astro-ph/9911449)
Blain A. W., Kneib J.-P., Ivison R. J., Smail I., 1999, ApJ, 512, L87
Borys C., Chapman S., Halpern M., Scott D., 2002, MNRAS, 330, 63
Carilli C. L., Owen F., Yun M., Bertoldi F., Bertarini A., Menten K. M., Kreysa E., Zylka R., 2000, in Lowenthal J. D., Hughes D. H., eds, Deep Millimeter Surveys, Implications for Galaxy Formation and Evolution. World Scientific, Singapore, p. 27
Cesarsky C. J., Abergel A., Agnese P. et al., 1996, A&A, 315, 32
Chapman S. C., Scott D., Steidel C. et al., 2000, MNRAS, 319, 318
Chapman S. C., Lewis G. F., Helou G., 2002a, ApJ, submitted
Chapman S. C., Smail I., Ivison R. J., Helou G., Dale D. A., Lagache G., 2002b, ApJ, 573, 66
Charry R., Elbaz D., 2001, ApJ, 556, 562
Clements C., Désert F. X., Franceschini A., Reach W. T., Baker A. C., Davies J. K., Cesarscky C., 1999, A&A, 346, 383
Cohen J., Hogg D. W., Blandford R., Cowie L. L., Hu E., Songaila A., Shopbell S., Richberg K., 2000, ApJ, 538, 29
Cox P., Omont A., Djorgovski S. G. et al., 2002, A&A, 387, 406
Dale D., Helou G., Contursi A., Silbermann N. A., Kolhatkar S., 2001, ApJ, 549, 215
de Bernardis P., Ade P. A. R., Bock J. J. et al., 2002, ApJ, 564, 559
Désert F. X., Boulanger F., Puget J-.L., 1990, A&A, 327, 215
Devriendt J. E. G., Guiderdoni B., 2000, A&A, 363, 851
Dole H., Gispert R., Lagache G. et al., 2000, in Lemke D., Stickel M., Wilke K., eds, Springer Lecture Notes in Physics, ISO Surveys of a Dusty Universe. Springer-Verlag, Berlin, p. 54 (astro-ph/0002283)
Dole H., Gispert R., Lagache G. et al., 2001, A&A, 372, 364
Dole H., Lagache G., Puget J.-L., 2002, ApJ, in press
Dunne L., Eales S. A., 2001, MNRAS, 327, 697
Dunne L., Eales S. A., Michael E., Ivison R., Alexander P., Clements D. L., 2000, MNRAS, 315, 115
Dwek E., Arendt R. G., Hauser M. G. et al., 1998, ApJ, 508, 106
Eales S., Lilly S., Walter G., Dunne L., Bond J. R., Hammer F., Le Fevre D., Crampton D., 1999, ApJ, 515, 518
Eales S., Lilly S., Webb T., Dunne L., Gear W., Clements D., Yun M., 2000, AJ, 120, 2244
Elbaz D., Cesarsky C. J., Fadda D. et al., 1999, A&A, 351, 37
Elbaz D., Cesarsky C. J., Chanial P., Aussel M., Franceschini A., Fadda D., Chary R. R., 2002, A&A, 384, 848
Ellis R. S., 1997, ARA&A, 35, 389
Fabian A. C., Smail I., Iwasawa K. et al., 2000, MNRAS, 315, 8
Fadda D., Flores H., Hasinger G., Franceschini A., Altieri B., Cesarsky C. J., Elbaz D., Ferrando P., 2002, A&A, 383, 838
Finkbeiner D. P., Davis M., Schlegel D. J., 2000, ApJ, 544, 81
Fixsen D. J., Dwek E., Mather J. C., Bennett C. L., Schafer R. A., 1998, ApJ, 508, 123
Flores H., Hammer F., Désert F.-X. et al., 1999a, A&A, 343, 389
Flores H., Hammer F., Thuan T. X. et al., 1999b, ApJ, 517, 148
Ford H. C., Tsvetanov Z. I., Ferrarese L., Jaffe W., 1998, in Sofue Y., ed., Proc. IAU Symp. 184, The Central Regions of the Galaxy and Galaxies. Kluwer, Dordrecht
Franceschini A., Andreani P., Danese L., 1998, MNRAS, 296, 709
Franceschini A., Aussel H., Césarsky C. J., Elbaz D., Fadda D., 2001, A&A, 378, 1
Freedman W. L., Madore B. F., Gibson B. K. et al., 2001, ApJ, 553, 47
Gispert R., Lagache G., Puget J.-L., 2000, A&A, 360, 1
Glenn J., Bock J. J., Chattopadhyay G. et al., 1998, SPIE, 3357, 326
Gregorich D. T., Neugebauer G., Soifer B. T., Gunn J. E., Herter T. L., 1995, AJ, 110, 259
Guiderdoni B., 2001, in Combes F., Barret D., Thévenin F., eds, SF2 A-2001; Semaine de l'Astrophysique Francaise. EdP-Sciences, p. 259
Guiderdoni B., Hivon E., Bouchet F., Maffei B., 1998, MNRAS, 295, 877
Hacking P. B., Houck J. R., 1987, ApJS, 63, 311
Hatton S., Devriendt J. E. G., Ninin S., Bouchet F. R., Guiderdoni B., Vibert D., 2002, MNRAS, in press
Hauser M. G., Dwek E., 2001, ARA&A, 37, 249
Hauser M. G., Arendt R. G., Kelsall T. et al., 1998, ApJ, 508, 25
Helou G., 2000, in Casoli F., Lequeux J., David F., eds, Les Houches, Session LXX, Infrared Space Astronomy, Today and Tomorrow. Published in cooperation with NATO Scientific Affairs. Springer-Verlag, Berlin, p.337
Holland W. S., Cunningham C. R., Gear W. K. et al., 1998, SPIE, 3357, 305
Holland W. S., Duncan W. D., Audley M. D. et al., 2001, AAS Meeting 199, #103.06
Hornschemeier A. E., Brandt W. N., Garmire G. P. et al., 2000, ApJ, 541, 49
Hughes D. H., Dunlop J. S., Rowan-Robinson M. et al., 1998, Nat, 394, 241
Juvela M., Mattila K., Lemke D., 2000, A&A, 360, 813
Kakazu Y., Sanders D. B., Joseph R. D. et al., 2002, astro-ph/0201326
Kawara K., Sato Y., Matsuhara H. et al., 1998, A&A, 336, L9
Kessler M. F., Steinz J. A., Anderegg M. E. et al., 1996, A&A, 315, 27

Kim D.-C., Sanders D. B., 1998, ApJSS, 119, 41
Kiss Cs., Ábrahém P., Klaas U., Juvela M., Lemke D., 2001, A&A, 379, 1161
Klaas U., Haas M., Muller S. A. H. et al., 2001, A&A, 379, 823
Knox L., Cooray A., Eisenstein D., Haiman Z., 2001, ApJ, 550, 7
Lagache G., Puget J.-L., 2000, A&A, 355, 17
Lagache G., Abergel A., Boulanger F., Désert F., Suget J.-L., 1999, A&A, 344, 322
Lagache G., Haffner L. M., Reynolds R. J., Tufte S. L., 2000, A&A, 354, 247
Lanzetta K. M., Yahata N., Pascarelle S., Chen H.-W., Fernéndez-Soto A., 2002, ApJ, 570, 492
Leisawitz D. et al., 2001, in Woodward C. E., Bicay M. D., Shull J. M., eds, ASP Conf. Ser. Vol. 231, Tetons 4, Galactic Structure, Stars and the Interstellar Medium. Astron. Soc. Pac., San Francisco, p. 639
Lemke D., Klaas U., Abolins J. et al., 1996, A&A, 315, 64
Lilly S. J., Eales S. A., Gear W. K. P., Hammer F., Le Févre D., Crampton D., Bond J. R., Dunne L., 1999, ApJ, 518, 641
Linden-Vornle M. J. D., Norgaard-Nielsen H. U., Jorgensen H. E. et al., 2000, A&A, 353, L51
Lonsdale C. J., Hacking P. B., Conrow T. B., Rowan-Robinson M., 1990, ApJ, 358, 20
Lutz D., Genzel R., Kunze D., Rigopoulou D., Spoon H. W. W., Sturm E., Train D., Moorwood A. F. M., 1999, Ap&SS, 266, 85
Maffei B., 1994, PhD thesis, Institut d'Astrophysique Spatiale
Malkan M. A., Stecker F. W., 2001, ApJ, 555, 641
Matsuhara H., Kawara K., Sato Y. et al., 2000, A&A, 361, 407
Metcalfe L., 2000, in Harwit M., Hauser M. G., eds, Proc. IAU Symp. 204, The Extragalactic Infrared Background and Its Cosmological Implications. Astron. Soc. Pac., San Francisco, p. 18
Miville-Deschênes M.-A., Lagache G., Puget J.-L., 2002, A&A, 393, 749
Page M. J., Stevens J. A., Mittaz J. P. D., Carrera F. J., 2002, Sci, 294, 2516 (astro-ph/0202102)
Patris J., Dennefeld M., Lagache G., Dole H., 2002, A&A, submitted
Pearson C. P., 2001, MNRAS, 325, 1511
Perlmutter S., Aldering G., Goldhaber G. et al., 1999, ApJ, 517, 565
Perrotta F., Baccigalupi C., Bartelman M., De Zotti G., Granato G. L., MNRAS, 329, 445
Pilbratt G. L., 2001, in Pilbratt G. L., Cernicharo J., Heras A. M., Prusti T., Harris R., eds, Proc. Symp. on the Promise of the Herschel Space Observatory, Toledo, Spain, 2000 December 12–15. ESA SP-460, pp. 13–20
Poggianti B. M., Wu H., 2000, ApJ, 529, 157
Poggianti B. M., Smail I., Dressler A., Couch V. J., Barger M. J., Butcher M., Ellis R. J., Oemler A. J., 1999, ApJ, 518, 576
Poggianti B. M., Bressan A., Franceschini A., 2001, ApJ, 550, 195
Puget J.-L., Abergel A., Bernard J.-P., Boulanger F., Burton W. B., Desert F. X., Martmann D., 1996, A&A, 308, L5
Puget J. L., Lagache G., Clements D. L. et al., 1999, A&A, 354, 29
Renault C., Barrau A., Lagache G., Puget J.-L., 2001, A&A, 371, 771
Rigopoulou D., Franceschini A., Aussel H. et al., 2000, ApJ, 537, 85
Rowan-Robinson M., 2001, ApJ, 549, 745
Rowan-Robinson M., Hughes J., Vedi K., Walker D. W., 1990, MNRAS, 289, 490
Sajina A., Borys C., Chapman S., Dale H., Halpern M., Lagache G., Puget J. L., Scott D., 2002, submitted
Sanders D. B., Mirabel I. F., 1996, ARA&A, 34, 749
Saunders W., Rowan-Robinson M., Lawrence A., Efstathiou G., Kaiser N., Ellis R. S., Frenk C. S., 1990, MNRAS, 242, 318
Schlegel D. J., Finkbeiner D. P., Davis M., 1998, ApJ, 500, 525
Scott S. E., Fox M. J., Dunlop J. S. et al., 2002, MNRAS, 331, 817
Serjeant S., Efstathiou A., Oliver S. et al., 2001, MNRAS, 322, 262
Serra G., Puget J.-L., Ryter C. E., Wijnbergen J. J., 1978, ApJ, 222, 21
Severgnini P., Maiolino R., Salvati M. et al., 2000, A&A, 360, 457
Silverberg R. F., Hauser M. G., Mather J. C., Gezari D. Y., Kelsall T., Cheung L. H., 1979, SPIE, 172, 149
Smail I., Ivison R. J., Blain A. W., 1997, ApJ, 490, L5
Smail I., Ivison R. J., Blain A. W., Kneib J.-P., 1998, ApJ, 507, 21
Soifer B. T., Neugebauer G., 1991, AJ, 101, 354
Stickel M., Bogun S., Lemke D. et al., 1998, A&A, 336, 116
Stickel M., Lemke D., Klaas U. et al., 2000, A&A, 359, 865
Takeuchi T. T., Ishii T. T., Hirashita H., Yoshikawa K., Matsukara H., Kawara K., Okude H., 2001, PASJ, 53, 37
Trentham N., Kormendy J., Sanders D. B., 1999, AJ, 117, 2152
Veilleux S., Kim D.-C., Sanders D. B., 1999, ApJ, 522, 113
Wang Y. P., 2002, A&A, 383, 755
Wang Y. P., Biermann P. L., 2000, A&A, 356, 808
Webb T. M. A., Eales S. A., Lilly S. J., Clements D. L., Dunne L., Gear W. K., Florès H., Yun M., 2002, ApJ, submitted
Xu C., Lonsdale C. J., Shupe D. L., O'Linger J. A., Mesin F., 2001, 562, 179

APPENDIX A: ELECTRONIC DISTRIBUTION

We provide, in an electronic form through a web page,[8] a distribution of the model's outputs and programs (to be used in IDL) containing:

(i) The array $\mathrm{d}N/(\mathrm{d}\ln L\,\mathrm{d}z)$ as a function of L and z, $\mathrm{d}S/\mathrm{d}z$ as a function of L and z, and S_ν in Jy for each luminosity and redshift, from 10 to 2000 μm and the evolution of the LF for both the normal and the starburst populations (for $\Omega_\Lambda = 0.7$, $\Omega_0 = 0.3$ and $h = 0.65$).

(ii) Some useful programs that compute the integral counts, detected sources, CIB and fluctuation redshift distribution, and the level of the fluctuations from the previous data cubes.

This paper has been typeset from a TEX/LATEX file prepared by the author.

[8] http://www.ias.fr/PPERSO/glagache/act/gal_model.html